Eur. Phys. J. C 4, 367–385 (1998)
DOI 10.1007/s100529800903

THE EUROPEAN PHYSICAL JOURNAL C

Study of B_s^0 oscillations and lifetime using fully reconstructed D_s^- decays

The ALEPH Collaboration

R. Barate, D. Buskulic, D. Decamp, P. Ghez, C. Goy, J.-P. Lees, A. Lucotte, M.-N. Minard, J.-Y. Nief, B. Pietrzyk
Laboratoire de Physique des Particules (LAPP), IN^{2}P^3-CNRS, F-74019 Annecy-le-Vieux Cedex, France

G. Boix, M.P. Casado, M. Chmeissani, J.M. Crespo, M. Delfino, E. Fernandez, M. Fernandez-Bosman, Ll. Garrido,[15] E. Graugès, A. Juste, M. Martinez, G. Merino, R. Miquel, Ll.M. Mir, I.C. Park, A. Pascual, J.A. Perlas, I. Riu, F. Sanchez
Institut de Física d'Altes Energies, Universitat Autònoma de Barcelona, E-08193 Bellaterra (Barcelona), Spain[7]

A. Colaleo, D. Creanza, M. de Palma, G. Gelao, G. Iaselli, G. Maggi, M. Maggi, S. Nuzzo, A. Ranieri, G. Raso, F. Ruggieri, G. Selvaggi, L. Silvestris, P. Tempesta, A. Tricomi,[3] G. Zito
Dipartimento di Fisica, INFN Sezione di Bari, I-70126 Bari, Italy

X. Huang, J. Lin, Q. Ouyang, T. Wang, Y. Xie, R. Xu, S. Xue, J. Zhang, L. Zhang, W. Zhao
Institute of High-Energy Physics, Academia Sinica, Beijing, The People's Republic of China[8]

D. Abbaneo, R. Alemany, U. Becker, P. Bright-Thomas, D. Casper, M. Cattaneo, F. Cerutti, V. Ciulli, G. Dissertori, H. Drevermann, R.W. Forty, M. Frank, R. Hagelberg, J.B. Hansen, J. Harvey, P. Janot, B. Jost, I. Lehraus, P. Mato, A. Minten, L. Moneta,[25] A. Pacheco, J.-F. Pusztaszeri,[23] F. Ranjard, L. Rolandi, D. Rousseau, D. Schlatter, M. Schmitt, O. Schneider, W. Tejessy, F. Teubert, I.R. Tomalin, H. Wachsmuth, A. Wagner[20]
European Laboratory for Particle Physics (CERN), CH-1211 Geneva 23, Switzerland

Z. Ajaltouni, F. Badaud, G. Chazelle, O. Deschamps, A. Falvard, C. Ferdi, P. Gay, C. Guicheney, P. Henrard, J. Jousset, B. Michel, S. Monteil, J-C. Montret, D. Pallin, P. Perret, F. Podlyski, J. Proriol, P. Rosnet
Laboratoire de Physique Corpusculaire, Université Blaise Pascal, IN^{2}P^3-CNRS, Clermont-Ferrand, F-63177 Aubière, France

T. Fearnley, J.D. Hansen, J.R. Hansen, P.H. Hansen, B.S. Nilsson, B. Rensch, A. Wäänänen
Niels Bohr Institute, DK-2100 Copenhagen, Denmark[9]

G. Daskalakis, A. Kyriakis, C. Markou, E. Simopoulou, I. Siotis, A. Vayaki
Nuclear Research Center Demokritos (NRCD), GR-15310 Attiki, Greece

A. Blondel, G. Bonneaud, J.-C. Brient, P. Bourdon, A. Rougé, M. Rumpf, A. Valassi,[6] M. Verderi, H. Videau
Laboratoire de Physique Nucléaire et des Hautes Energies, Ecole Polytechnique, IN^{2}P^3-CNRS, F-91128 Palaiseau Cedex, France

T. Boccali, E. Focardi, G. Parrini, K. Zachariadou
Dipartimento di Fisica, Università di Firenze, INFN Sezione di Firenze, I-50125 Firenze, Italy

M. Corden, C. Georgiopoulos, D.E. Jaffe
Supercomputer Computations Research Institute, Florida State University, Tallahassee, FL 32306-4052, USA [13,14]

A. Antonelli, G. Bencivenni, G. Bologna,[4] F. Bossi, P. Campana, G. Capon, V. Chiarella, G. Felici, P. Laurelli, G. Mannocchi,[5] F. Murtas, G.P. Murtas, L. Passalacqua, M. Pepe-Altarelli
Laboratori Nazionali dell'INFN (LNF-INFN), I-00044 Frascati, Italy

L. Curtis, S.J. Dorris, A.W. Halley, J.G. Lynch, P. Negus, V. O'Shea, C. Raine, J.M. Scarr, K. Smith, P. Teixeira-Dias, A.S. Thompson, E. Thomson, F. Thomson
Department of Physics and Astronomy, University of Glasgow, Glasgow G12 8QQ,United Kingdom[10]

O. Buchmüller, S. Dhamotharan, C. Geweniger, G. Graefe, P. Hanke, G. Hansper, V. Hepp, E.E. Kluge, A. Putzer, J. Sommer, K. Tittel, S. Werner, M. Wunsch
Institut für Hochenergiephysik, Universität Heidelberg, D-69120 Heidelberg, Germany[16]

R. Beuselinck, D.M. Binnie, W. Cameron, P.J. Dornan, M. Girone, S. Goodsir, E.B. Martin, N. Marinelli, A. Moutoussi, J. Nash, J.K. Sedgbeer, P. Spagnolo, M.D. Williams
Department of Physics, Imperial College, London SW7 2BZ, United Kingdom[10]

V.M. Ghete, P. Girtler, E. Kneringer, D. Kuhn, G. Rudolph
Institut für Experimentalphysik, Universität Innsbruck, A-6020 Innsbruck, Austria[18]

A.P. Betteridge, C.K. Bowdery, P.G. Buck, P. Colrain, G. Crawford, A.J. Finch, F. Foster, G. Hughes, R.W.L. Jones, M.I. Williams
Department of Physics, University of Lancaster, Lancaster LA1 4YB, United Kingdom[10]

I. Giehl, A.M. Greene, C. Hoffmann, K. Jakobs, K. Kleinknecht, G. Quast, B. Renk, E. Rohne, H.-G. Sander, P. van Gemmeren, C. Zeitnitz
Institut für Physik, Universität Mainz, D-55099 Mainz, Germany[16]

J.J. Aubert, C. Benchouk, A. Bonissent, G. Bujosa, J. Carr, P. Coyle, F. Etienne, O. Leroy, F. Motsch, P. Payre, M. Talby, A. Sadouki, M. Thulasidas, K. Trabelsi
Centre de Physique des Particules, Faculté des Sciences de Luminy, IN^2P^3-CNRS, F-13288 Marseille, France

M. Aleppo, M. Antonelli, F. Ragusa
Dipartimento di Fisica, Università di Milano e INFN Sezione di Milano, I-20133 Milano, Italy

R. Berlich, W. Blum, V. Büscher, H. Dietl, G. Ganis, C. Gotzhein, H. Kroha, G. Lütjens, G. Lutz, C. Mannert, W. Männer, H.-G. Moser, R. Richter, A. Rosado-Schlosser, S. Schael, R. Settles, H. Seywerd, H. Stenzel, W. Wiedenmann, G. Wolf
Max-Planck-Institut für Physik, Werner-Heisenberg-Institut, D-80805 München, Germany[p]

J. Boucrot, O. Callot,[2] S. Chen, Y. Choi,[21] A. Cordier, M. Davier, L. Duflot, J.-F. Grivaz, Ph. Heusse, A. Höcker, A. Jacholkowska, D.W. Kim,[12] F. Le Diberder, J. Lefrançois, A.-M. Lutz, I. Nikolic, M.-H. Schune, E. Tournefier, J.-J. Veillet, I. Videau, D. Zerwas
Laboratoire de l'Accélérateur Linéaire, Université de Paris-Sud, IN^2P^3-CNRS, F-91405 Orsay Cedex, France

P. Azzurri, G. Bagliesi,[2] G. Batignani, S. Bettarini, C. Bozzi, G. Calderini, M. Carpinelli, M.A. Ciocci, R. Dell'Orso, R. Fantechi, I. Ferrante, L. Foà,[1] F. Forti, A. Giassi, M.A. Giorgi, A. Gregorio, F. Ligabue, A. Lusiani, P.S. Marrocchesi, A. Messineo, F. Palla, G. Rizzo, G. Sanguinetti, A. Sciabà, J. Steinberger, R. Tenchini, G. Tonelli,[19] C. Vannini, A. Venturi, P.G. Verdini
Dipartimento di Fisica dell'Università, INFN Sezione di Pisa, e Scuola Normale Superiore, I-56010 Pisa, Italy

G.A. Blair, L.M. Bryant, J.T. Chambers, M.G. Green, T. Medcalf, P. Perrodo, J.A. Strong, J.H. von Wimmersperg-Toeller
Department of Physics, Royal Holloway & Bedford New College, University of London, Surrey TW20 OEX, United Kingdom[10]

D.R. Botterill, R.W. Clifft, T.R. Edgecock, S. Haywood, P.R. Norton, J.C. Thompson, A.E. Wright
Particle Physics Dept., Rutherford Appleton Laboratory, Chilton, Didcot, Oxon OX11 OQX, United Kingdom[10]

B. Bloch-Devaux, P. Colas, S. Emery, W. Kozanecki, E. Lançon, M.-C. Lemaire, E. Locci, P. Perez, J. Rander, J.-F. Renardy, A. Roussarie, J.-P. Schuller, J. Schwindling, A. Trabelsi, B. Vallage
CEA, DAPNIA/Service de Physique des Particules, CE-Saclay, F-91191 Gif-sur-Yvette Cedex, France[17]

S.N. Black, J.H. Dann, R.P. Johnson, H.Y. Kim, N. Konstantinidis, A.M. Litke, M.A. McNeil, G. Taylor
Institute for Particle Physics, University of California at Santa Cruz, Santa Cruz, CA 95064, USA[22]

C.N. Booth, C.A.J. Brew, S. Cartwright, F. Combley, M.S. Kelly, M. Lehto, J. Reeve, L.F. Thompson
Department of Physics, University of Sheffield, Sheffield S3 7RH, United Kingdom[10]

K. Affholderbach, A. Böhrer, S. Brandt, G. Cowan, C. Grupen, P. Saraiva, L. Smolik, F. Stephan
Fachbereich Physik, Universität Siegen, D-57068 Siegen, Germany[16]

M. Apollonio, L. Bosisio, R. Della Marina, G. Giannini, B. Gobbo, G. Musolino
Dipartimento di Fisica, Università di Trieste e INFN Sezione di Trieste, I-34127 Trieste, Italy

J. Rothberg, S. Wasserbaech
Experimental Elementary Particle Physics, University of Washington, WA 98195 Seattle, USA

S.R. Armstrong, E. Charles, P. Elmer, D.P.S. Ferguson, Y. Gao, S. González, T.C. Greening, O.J. Hayes, H. Hu, S. Jin, P.A. McNamara III, J.M. Nachtman,[24] J. Nielsen, W. Orejudos, Y.B. Pan, Y. Saadi, I.J. Scott, J. Walsh, Sau Lan Wu, X. Wu, J.M. Yamartino, G. Zobernig
Department of Physics, University of Wisconsin, Madison, WI 53706, USA[11]

Received: 12 December 1997 / Revised version: 24 February 1998 / Published online: 23 June 1998

Abstract. A search for B_s^0 oscillations is performed using approximately 4 million $Z \to q\bar{q}$ events collected by the ALEPH experiment during 1991–1995. B_s^0 candidates are partially reconstructed by combining tracks with fully reconstructed D_s^- candidates. The B_s^0 production flavour is estimated from the sign of the opposite hemisphere charge, a fragmentation kaon in the same hemisphere, or a lepton in the opposite hemisphere. From a total sample of 1620 candidates, with a B_s^0 purity estimated to be 22%, all values of Δm_s below $3.9\,\mathrm{ps}^{-1}$ and between 6.5 and $8.8\,\mathrm{ps}^{-1}$ are excluded at 95% CL. From the same sample, the B_s^0 lifetime is measured to be $\tau_s = 1.47 \pm 0.14(\mathrm{stat}) \pm 0.08(\mathrm{syst})\,\mathrm{ps}$. This analysis selects mainly hadronic B_s^0 decays and is statistically independent of a previous ALEPH analysis selecting $B_s^0 \to D_s^{(*)-}\ell^+\nu$ candidates. Combining these two analyses yields $\Delta m_s > 7.9\,\mathrm{ps}^{-1}$ at 95% CL and $\tau_s = 1.51 \pm 0.11\,\mathrm{ps}$.

1 Introduction

Transitions between the B_s^0 and $\bar{B}_s^0$ states result in oscillations with a frequency Δm_s related to the mass difference between the mass eigenstates of the $B_s^0 - \bar{B}_s^0$ system. The Standard Model predictions for Δm_s and Δm_d, the $B_d^0 - \bar{B}_d^0$ oscillation frequency, are derived from calculations of box diagrams where top quark exchange dominates. Uncertainties due to non-perturbative QCD correction factors partially cancel in the frequency ratio, yielding

$$\frac{\Delta m_s}{\Delta m_d} = \frac{m_{B_s^0}}{m_{B_d^0}} \xi_s^2 \left| \frac{V_{ts}}{V_{td}} \right|^2 , \quad (1)$$

where V_{ts} and V_{td} are elements of the Cabibbo-Kobayashi-Maskawa quark mixing matrix. The quantity ξ_s, equal to unity up to SU(3) symmetry breaking factors, is estimated to be 1.14 ± 0.08 after corrections [1]. A measurement of the ratio $\Delta m_s/\Delta m_d$ would therefore allow the extraction of $|V_{ts}/V_{td}|$.

As the ratio $|V_{ts}/V_{td}|$ is expected to be large, the B_s^0 oscillation frequency is thought to be much higher than the well measured B_d^0 oscillation frequency [2]. As yet, various analyses to search for B_s^0 oscillations at LEP [3–8] have failed to directly observe significant B_s^0 oscillations.

The highest published lower limit on Δm_s is $6.6\,\mathrm{ps}^{-1}$ at 95% CL [5]. It was obtained by ALEPH using data recorded in 1991–1995. This gave a sample of 277 fully reconstructed D_s^- candidates correlated with an oppositely charged lepton in the same hemisphere and attributed to $B_s^0 \to D_s^{(*)-} \ell^+ \nu$ decays. This demonstrated that the use of fully reconstructed D_s^- mesons is competitive with more inclusive analyses, the small size of the event sample being compensated by the significantly improved B_s^0 purity and proper time resolution.

In this paper, a new and complementary search for B_s^0 oscillations and a measurement of the B_s^0 lifetime are presented, which also use fully reconstructed D_s^- candidates in the ALEPH data collected during 1991–1995. The selected signal consists mainly of hadronic $B_s^0 \to D_s^-$ decays and is statistically independent of the D_s^--lepton analysis [5]. The following channels are considered[1]:

[1] Now at CERN, 1211 Geneva 23, Switzerland
[2] Also at CERN, 1211 Geneva 23, Switzerland
[3] Also at Dipartimento di Fisica, INFN, Sezione di Catania, Catania, Italy
[4] Also Istituto di Fisica Generale, Università di Torino, Torino, Italy
[5] Also Istituto di Cosmo-Geofisica del C.N.R., Torino, Italy
[6] Supported by the Commission of the European Communities, contract ERBCHBICT941234
[7] Supported by CICYT, Spain
[8] Supported by the National Science Foundation of China
[9] Supported by the Danish Natural Science Research Council
[10] Supported by the UK Particle Physics and Astronomy Research Council
[11] Supported by the US Department of Energy, grant DE-FG0295-ER40896
[12] Permanent address: Kangnung National University, Kangnung, Korea
[13] Supported by the US Department of Energy, contract DE-FG05-92ER40742
[14] Supported by the US Department of Energy, contract DE-FC05-85ER250000
[15] Permanent address: Universitat de Barcelona, 08208 Barcelona, Spain
[16] Supported by the Bundesministerium für Bildung, Wissenschaft, Forschung und Technologie, Germany
[17] Supported by the Direction des Sciences de la Matière, C.E.A
[18] Supported by Fonds zur Förderung der wissenschaftlichen Forschung, Austria
[19] Also at Istituto di Matematica e Fisica, Università di Sassari, Sassari, Italy
[20] Now at Schweizerischer Bankverein, Basel, Switzerland
[21] Permanent address: Sung Kyun Kwan University, Suwon, Korea
[22] Supported by the US Department of Energy, grant DE-FG03-92ER40689
[23] Now at School of Operations Research and Industrial Engineering, Cornell University, Ithaca, NY 14853-3801, USA
[24] Now at University of California at Los Angeles (UCLA), Los Angeles, CA 90024, USA
[25] Now at University of Geneva, 1211 Geneva 4, Switzerland

[1] Charge conjugate modes are assumed throughout. The notations ϕ, K^{*0} and ρ^- are used for $\phi(1020)$, $K^*(892)^0$ and $\rho(770)^-$ respectively. Lepton (ℓ) means muon or electron. The generic notation "$D_s^- \to \phi\,\rho^-$" includes both two-body $D_s^- \to \phi\,\rho^-$ decays followed by $\rho^- \to \pi^-\pi^0$ and non-resonant three-body $D_s^- \to \phi\,\pi^-\pi^0$ decays. The generic notation "$B_s^0 \to D_s^- + X$" includes direct $B_s^0 \to D_s^- + X$ decays, $B_s^0 \to D_s^{*-} + X$ decays followed by $D_s^{*-} \to D_s^-\gamma$ or

$B_s^0 \to D_s^- + \text{hadron(s)}$, $D_s^- \to \phi\pi^-$, $\phi \to K^+K^-$;
$B_s^0 \to D_s^- + \text{hadron(s)}$, $D_s^- \to K^{*0}K^-$, $K^{*0} \to K^+\pi^-$;
$B_s^0 \to D_s^- + \text{hadron}$, $D_s^- \to K^0K^-$, $K_S^0 \to \pi^+\pi^-$;
$B_s^0 \to D_s^- + \text{hadron}$, $D_s^- \to \phi\ell^-\bar{\nu}$, $\phi \to K^+K^-$;
$B_s^0 \to D_s^- + \text{lepton}$, $D_s^- \to \phi\rho^-$, $\phi \to K^+K^-$, $\rho^- \to \pi^-\pi^0$, $\pi^0 \to \gamma\gamma$.

As a semileptonic B_s^0 decay is not required (except for the $D_s^- \to \phi\rho^-$ channel), the samples are larger than those used in the D_s^--lepton analysis. For the same reason their purity is lower as they suffer from additional and more copious background components, in particular D_s^- from $Z \to c\bar{c}$ and events in which a hadron from the primary vertex is associated with a D_s^- from $Z \to b\bar{b}$ to form a B_s^0 candidate. Overall, this analysis is less powerful than the D_s^--lepton analysis, but a significant improvement in sensitivity is found when the two analyses are combined.

This paper is organized in the following way. After a brief description of the ALEPH apparatus, the event selection is described in Sect. 3 and the determination of the composition of the selected samples in Sect. 4. The next two sections explain how the B_s^0 proper time and initial state are estimated; this information is then used to construct the likelihood of the selected samples (Sect. 7). The results are presented and discussed in Sects. 8 and 9. Finally the combination with the D_s^--lepton analysis is presented in Sect. 10.

2 The ALEPH detector

The ALEPH detector and its performance from 1991 to 1995 are described in detail elsewhere [9,10], and only a brief overview of the apparatus is given here. Surrounding the beam pipe, a high resolution vertex detector (VDET) consists of two layers of double-sided silicon microstrip detectors, positioned at average radii of 6.5 cm and 11.3 cm, and covering respectively 85% and 69% of the solid angle. The spatial resolution for the $r\phi$ and z projections (transverse to and along the beam axis, respectively) is 12 μm at normal incidence. The vertex detector is surrounded by a drift chamber with eight coaxial wire layers with an outer radius of 26 cm and by a time projection chamber (TPC) that measures up to 21 three-dimensional points per track at radii between 30 cm and 180 cm. These detectors are immersed in an axial magnetic field of 1.5 T and together measure the momenta of charged particles with a resolution $\sigma(p)/p = 6 \times 10^{-4}\, p_T \oplus 0.005$ (p_T in GeV/c). The resolution of the three-dimensional impact parameter in the transverse and longitudinal view for tracks having information from all tracking detectors and two VDET hits (a VDET "hit" being defined as having information from both the $r\phi$ and z views) can be parametrized as $\sigma = 25\,\mu\text{m} + 95\,\mu\text{m}/p$ (p in GeV/c). The TPC also provides up to 338 measurements of the specific ionization of a charged particle. In the following, the dE/dx information is considered as available if more than 50 samples are present. Particle identification is based on the dE/dx estimators $\chi_{\pi,K} = (I - I^{\text{exp}}_{\pi,K})/\sigma_I$, where I is the measured ionization, $I^{\text{exp}}_{\pi,K}$ the expected ionization for the π or K mass hypothesis, and σ_I the expected resolution on I. The TPC is surrounded by a lead/proportional-chamber electromagnetic calorimeter segmented into $0.9^\circ \times 0.9^\circ$ projective towers and read out in three sections in depth, with energy resolution $\sigma(E)/E = 0.18/\sqrt{E} + 0.009$ (E in GeV). The iron return yoke of the magnet is instrumented with streamer tubes to form a hadron calorimeter, with a thickness of over 7 interaction lengths and is surrounded by two additional double-layers of streamer tubes to aid muon identification. An algorithm combines all these measurements to provide a determination of the energy flow [10] with an uncertainty on the measurable total energy of $\sigma(E) = (0.6\sqrt{E/\text{GeV}} + 0.6)\,\text{GeV}$.

3 Event selection

This analysis uses approximately 4 million hadronic events recorded by the ALEPH detector from 1991 to 1995 at centre of mass energies close to the Z mass, and selected with the charged particle requirements described in [11]. It also relies on Monte Carlo samples of fully simulated $Z \to q\bar{q}$ events, as well as D_s^- events from all sources. The Monte Carlo generator is based on JETSET 7.4 [12] with updated branching ratios; the Körner-Schuler model [13] is used for semileptonic b hadron decays.

The interaction point is reconstructed on an event-by-event basis using the constraint of the average beam spot position and envelope [14]. The average resolution is 85 μm for $Z \to b\bar{b}$ events, projected along the sphericity axis of the event.

The D_s^- reconstruction and selection is performed in the five channels listed in Sect. 1, using only tracks with at least four TPC hits and well within the detector acceptance ($|\cos\theta| < 0.95$, where θ is the angle with respect to the beam axis). The $D_s^- \to \phi\rho^-$ channel, involving the reconstruction of a π^0 and not considered in the previous D_s^--lepton analysis, suffers from a large combinatorial background and is only used here in correlation with an identified lepton to reconstruct B_s^0 candidates. The $D_s^- \to \phi\pi^-$, $D_s^- \to K^{*0}K^-$, $D_s^- \to K^0K^-$, and $D_s^- \to \phi\ell^-\bar{\nu}$ channels have already been exploited in the D_s^--lepton analysis, and the selected events are excluded from the present analysis. The remaining D_s^- candidates in these channels are combined with hadrons to form B_s^0 candidates. This is performed in two steps. First, each D_s^- candidate is vertexed with a single hadron track (subject to tight selection criteria) to form a B_s^0 vertex candidate. In the case that a good B_s^0 decay hadron is not found, a second attempt, using a more inclusive algorithm with relaxed cuts, allows several hadrons to be vertexed with the $D_s^- \to \phi\pi^-$ and $D_s^- \to K^{*0}K^-$ candidates. This "multi-hadron algorithm" is more efficient than the "single hadron algorithm" for hadronic $B_s^0 \to D_s^{\pm}$ decays; however, the increase in efficiency is larger for $\bar{b} \to W^+ \to D_s^+$ decays than for $\bar{b} \to D_s^-$ decays, because b hadron decays in

$D_s^{*-} \to D_s^-\pi^0$, and any other B_s^0 decays to excited states decaying strongly to a D_s^-

which the D_s^+ comes from a virtual W^+ yield more tracks on average. The samples selected with the multihadron algorithm have a lower B_s^0 purity, because of the increased efficiency for b hadrons other than B_s^0, and a worse charge correlation between the D_s^- and the b quark in the decaying B_s^0.

Overall, the event selection results in seven different samples, each containing D_s^- candidates reconstructed in a given channel and vertexed using a given algorithm to form B_s^0 candidates. The selection cuts, described in the following sections, are designed to select samples of D_s^- from B_s^0 decays statistically independent of that used in the D_s^--lepton analysis and tuned, on Monte Carlo events, to maximize the signal significance.

3.1 D_s^- selection in the $\phi\pi^-$, $K^{*0}K^-$, K^0K^- and $\phi\ell^-\bar{\nu}$ channels

To reconstruct the neutral daughter of the D_s^- ($\phi \to K^+K^-$, $K^{*0} \to K^+\pi^-$ or $K_S^0 \to \pi^+\pi^-$), pairs of oppositely charged tracks are required to come from a common vertex and to have a mass consistent with the nominal mass of a ϕ, K^{*0}, or K^0. A third track is then combined with each of these pairs to form a three-prong D_s^- vertex, except for the $D_s^- \to K^0K^-$ channel where the additional track is vertexed with the K^0 candidate to allow for separate D_s^- and K^0 vertices. For the $D_s^- \to K^{*0}K^-$ channel, this third track must have a charge opposite to that of the K^{*0} daughter assumed to be a kaon, and for the $D_s^- \to \phi\ell^-\bar{\nu}$ channel it is required to pass standard lepton identification cuts [15].

The cuts listed in Table 1 are applied in order to reduce the background. The K^0 selection is enhanced by requiring the pion candidates to be incompatible with originating from the primary vertex, the K^0 mass and vertex fit to yield a χ^2 per degree of freedom (χ^2/dof) less than 10, and the K^0 proper decay time to be larger than 1.5 mm/c. For all the charged kaon candidates, a cut is applied on the dE/dx information if available; $D_s^- \to K^{*0}K^-$ and $D_s^- \to K^0K^-$ candidates without dE/dx information for any of the charged kaon candidates are rejected. The probability that the hemisphere opposite to the D_s^- candidate arises from a light quark event is calculated from the track impact parameters with respect to the primary vertex (using the algorithm of [14]) and required to be small. Due to the spin structure of the $D_s^- \to \phi\pi^-$ and $D_s^- \to K^{*0}K^-$ decays, the helicity angle λ^*, defined as the angle between the charged daughter of the D_s^- and a kaon from the neutral daughter of the D_s^- in the rest frame of the neutral daughter, has a $\cos^2\lambda^*$ distribution. Since the background has a flatter distribution, the central part of that distribution is rejected. Finally, at least one of the tracks forming the D_s^- candidate is required to be associated with a VDET hit (in the $D_s^- \to K^0K^-$ case, the requirement applies to the K^- or to both pions of the K^0).

For the $D_s^- \to \phi\ell^-\bar{\nu}$ channel, the D_s^- mass and momentum are reconstructed assuming that the neutrino has an energy given by the measured missing energy in the hemisphere and the same direction as the $\phi\ell^-$ system; this results in a D_s^- mass resolution of approximately 230 MeV/c^2 with a central value shifted towards lower mass by ~ 250 MeV/c^2.

3.2 $B_s^0 \to D_s^-$+hadron(s) selection

A B_s^0 decay vertex candidate is formed by adding to a D_s^- candidate the highest momentum track X satisfying the following conditions:

- the charge of X is opposite to that of the D_s^-;
- the cosine of the angle between X and the D_s^- is greater than 0.8;
- the D_s^-+X vertex fit yields a χ^2 probability greater than 1%;
- the D_s^- decay length $\ell_{D_s^-}$, defined as the distance between the D_s^- and the D_s^-+X vertices projected along the D_s^- direction, satisfies $-0.2 < \ell_{D_s^-} < 2.0$ cm;
- the invariant mass of D_s^-+X is smaller than 5.5 GeV/c^2, and, for the $D_s^- \to \phi\ell^-\bar{\nu}$ channel only, larger than 1.8 GeV/c^2.

This algorithm is first applied with the additional requirement that X be an electron or muon identified using standard criteria [15]. If a candidate is found then the corresponding D_s^- candidate is rejected. The above algorithm is then applied again on the remaining D_s^- candidates to select $B_s^0 \to D_s^-$+single hadron candidates. The final cuts listed in Table 2 are then applied to these B_s^0 candidates; in addition $\ell_{D_s^-} > 0$ is required, and the hadron track is required to have a VDET hit and a momentum greater than 1.5 GeV/c.

Inefficiencies in the above single hadron vertexing algorithm are mainly due to cases where the leading track does not originate from the b hadron vertex. These cases can be recovered if lower momentum tracks are used in the vertex reconstruction. The multihadron vertexing algorithm described below is applied to the $D_s^- \to \phi\pi^-$ and $D_s^- \to K^{*0}K^-$ candidates that fail the tight single hadron vertexing, cannot be vertexed satisfactorily with any of the identified leptons in the event, and contain at least two tracks with a VDET hit.

For any such D_s^- candidate, each remaining charged track X of momentum greater than 0.7 GeV/c, with a VDET hit, and forming an angle with the D_s^- candidate whose cosine is greater than 0.8, is vertexed individually with the D_s^- candidate. Tracks yielding a vertex χ^2/dof in excess of 5 are rejected. A decay length is associated to each remaining track, which is calculated as the distance from the primary vertex to the D_s^-+X vertex projected on the axis of the closest jet (obtained using the JADE algorithm with $y_{\rm cut}$=0.02). A clustering algorithm is then applied to group tracks with similar decay lengths. Tracks originating from a b hadron are expected to cluster around the b hadron decay length, whereas tracks from the primary vertex either fail the χ^2 cut or result in a different decay length. Each cluster of tracks is then vertexed with the D_s^- candidate to form a B_s^0 vertex candidate. The total

Table 1. Cuts used to select D_s^- candidates. Subscript 1 (2) refers to the charged (neutral) daughter of the D_s^-; 3 and 4 refer to the daughters of 2, in order of decreasing mass

Requirement	$D_s^- \to \phi\pi^-$	$D_s^- \to K^{*0}K^-$	$D_s^- \to K^0K^-$	$D_s^- \to \phi\ell^-\bar{\nu}$
$p_{D_s^-} >$	10 GeV/c	12 GeV/c	5 GeV/c	–
$p_1 >$	2.5 GeV/c	3 GeV/c	3 GeV/c	3 GeV/c
$p_2 >$	5.5 GeV/c	4.5 GeV/c	–	10 GeV/c
$p_3 >$	1 GeV/c	2.5 GeV/c	–	2 GeV/c
$p_4 >$	1 GeV/c	1 GeV/c	–	2 GeV/c
$\max(p_3, p_4) >$	–	–	1.0 GeV/c	4.5 GeV/c
$\lvert m_{34} - m_2\rvert <$	7 MeV/c^2	25 MeV/c^2	12 MeV/c^2	5 MeV/c^2
D_s^- vertex χ^2/dof $<$	30	4	4	4
$N(K^\pm)$ with dE/dx info $\geq$	0 out of 2	1 out of 2	1 out of 1	0 out of 2
for each $K^\pm$, $\chi_\pi + \chi_K <$	1.6	1.6	-0.5	2.0
opp. hemi. prob(uds) $<$	–	0.3	0.3	0.1
$\lvert\cos\lambda^*\rvert >$	0.45	0.65	–	–

Table 2. Cuts used to select $B_s^0 \to D_s^-$+ single hadron candidates. The quantity θ^* is the angle between the hadron and the B_s^0 in the B_s^0 rest frame

Requirement	$D_s^- \to \phi\pi^-$	$D_s^- \to K^{*0}K^-$	$D_s^- \to K^0K^-$	$D_s^- \to \phi\ell^-\bar{\nu}$
if dE/dx avail, $\chi_\pi + \chi_K >$	-3.0	-1.0	-1.8	-3.0
B_s^0 vertex χ^2 prob $>$	1%	8%	4%	1%
mass (D_s^-,hadron) $>$	2.5 GeV/c	2.5 GeV/c	2.5 GeV/c	2.1 GeV/c
$p_{B_s^0} >$	23 GeV/c	27 GeV/c	27 GeV/c	30 GeV/c
$\lvert\cos\theta^*\rvert <$	0.9	0.7	0.9	1.0
B_s^0 decay length error $<$	0.04 cm	0.05 cm	0.10 cm	0.05 cm

charge of these B_s^0 candidates must not exceed two units in absolute value.

If more than one vertex candidate remains, the visible reconstructed mass (computed as the invariant mass of the D_s^- candidate and its associated tracks) and the separation from the primary vertex are used to select a solution. If the candidate with the highest reconstructed mass also has the largest separation from the primary vertex ($\sim 85\%$ of the cases, according to Monte Carlo studies), this candidate is chosen for the b hadron vertex. It corresponds to the true b hadron vertex in more than 95% of the simulated events. In the remaining cases ($\sim 15\%$), the vertex to which the highest momentum track is associated is chosen. Monte Carlo studies show that for this case the probability to select the correct B_s^0 vertex is about 80%. Finally, the B_s^0 vertex candidate is required to be reconstructed upstream of the D_s^- vertex, and the error on the B_s^0 decay length is required to be smaller than 400 μm.

3.3 $B_s^0 \to D_s^-$+lepton selection via $D_s^- \to \phi\rho^-$

A ϕ candidate is reconstructed using two oppositely charged tracks, with individual momenta greater than 1.5 GeV/c, and identified as kaons ($|\chi_K| < 2.0$) if dE/dx information is available. The K^+K^- system is required to have a momentum greater than 4.0 GeV/c and an invariant mass within 9 MeV/c^2 of the nominal ϕ mass.

The π^0 candidates are reconstructed using an algorithm involving a kinematic fit with the π^0 mass constraint [10]. The photons are required to have a minimum energy of 300 MeV each, a combined mass within 40 MeV/c^2 of the nominal π^0 mass, and a total momentum in excess of 1.5 GeV/c. The χ^2/dof of the kinematic fit is required to be less than 10. In order to form ρ^- candidates, each π^0 candidate is combined with a charged track of momentum greater than 0.5 GeV/c and identified as a pion ($|\chi_\pi| < 2.0$) if dE/dx information is available. The mass of the $\pi^0\pi^-$ system is required to lie within 150 MeV/c^2 of the nominal ρ^- mass. A D_s^- candidate is constructed from a ϕ and a ρ^-. At least two of the charged tracks making up the D_s^- candidate are required to have a VDET hit. A fit to the D_s^- decay vertex is performed; combinations with a vertex χ^2/dof < 10 are retained.

To construct a B_s^0 candidate the D_s^- candidates are combined with an oppositely charged lepton identified using standard criteria [15], and required to have a momentum of 3 GeV/c or more, a momentum transverse to the nearest jet of at least 0.75 GeV/c, and a VDET hit.

A second vertex fit is performed using the reconstructed D_s^- and the lepton candidate. The χ^2/dof of the vertex fit is required to be less than 5. The B_s^0 decay length is calculated as the distance between the primary event vertex and the $D_s^-\ell^+$ vertex projected on the axis of the jet nearest to the B_s^0 candidate. The B_s^0 vertex is required to lie upstream of the D_s^- decay vertex.

Finally, some further requirements are made upon the B_s^0 candidate to reduce combinatorial backgrounds. The B_s^0 momentum, reconstructed as the sum of the D_s^-, lep-

ton, and missing momentum in the B_s^0 hemisphere, is required to be greater than $25\,\mathrm{GeV}/c$. Furthermore the mass of the $D_s^-\ell^+$ system is required to lie between 2.5 and $5.5\,\mathrm{GeV}/c^2$, and that of the three charged tracks forming the D_s^- candidate is required to be below $1.75\,\mathrm{GeV}/c^2$. If after all cuts an event contains several candidates, that having the $\pi^0\pi^-$ mass closest to the nominal ρ^- mass is chosen; this is done in about 40% of the events.

4 Signal and background sources

The fraction of D_s^- events (and that of D^-, if appropriate) is determined in each sample from the data itself, by fitting the mass spectrum. These D_s^- and D^- events result from contributions of various physics processes; the amount of each of these contributions is determined from the physics parameters which control the corresponding process and from the reconstruction efficiency.

4.1 D_s^- mass fits

The D_s^- mass spectra after all the selection criteria described in Sect. 3 are shown in Fig. 1, separately for each of the seven samples. The superimposed curves represent fits to these mass distributions. The following sources of D_s^- candidates are considered:

- **True D_s^-:** the charged tracks used to reconstruct the D_s^- candidate are the products of a true D_s^- decay in the corresponding channel, and their mass assignment is correct. This source includes $D_s^- \to \phi\,\rho^-$ candidates where the π^0 is incorrectly reconstructed (either a fake π^0 or a true π^0 not from the $D_s^- \to \phi\,\rho^-$ decay).
- **True D^-:** the charged tracks used to reconstruct the D_s^- candidate are the products of a true D^- decay, and their mass assignment is correct. This source is only considered for the $\phi\pi^-$, K^0K^- and $\phi\rho^-$ channels. The D^- and D_s^- peaks may overlap only in the $\phi\rho^-$ mass spectrum, due to the poorer mass resolution.
- **D^- reflection:** the tracks used to reconstruct the D_s^- candidate are the products of a true D^- decay, but their mass assignment is wrong. This source is only considered for the $K^{*0}K^-$ channel, where a $D^- \to K^{*0}\pi^-$ decay can fake a $D_s^- \to K^{*0}K^-$ decay if the π^- is misidentified as a K^-. The D^- reflection has a significant overlap (in the $K^{*0}K^-$ mass spectrum) with the D_s^- peak. A possible D^- reflection in the K^0K^- channel is negligible because of the tight dE/dx requirement on the K^- candidate.
- **Combinatorial background:** the charged tracks used to reconstruct the D_s^- candidate do not all come from a common D_s^- or D^- decay, or their mass assignment is wrong (and they do not form a D^- reflection), or other additional particles are produced in the D_s^- or D^- decay.

In each sample, the combinatorial background is parametrized using a quadratic function with free parameters, except for the $D_s^- \to \phi\,\ell^-\bar{\nu}$ and $D_s^- \to \phi\,\rho^-$ channels where the shape of this background is taken from the Monte Carlo as it is not sufficiently constrained by the data sidebands. In all cases the normalisation of the combinatorial background is left free in the fit to the data.

For the $D_s^- \to \phi\,\pi^-$, $D_s^- \to K^0K^-$ and $D_s^- \to \phi\,\ell^-\bar{\nu}$ channels, a Gaussian parametrization of the D_s^- (and possible D^-) peaks is satisfactory; the width and central values of these Gaussian distributions are left free in the fit to the data.

For the $D_s^- \to \phi\,\rho^-$ channel, some true D_s^- and D^- events are reconstructed with the correct charged tracks, but a wrong π^0 candidate. These "wrong-π^0 events" have valid reconstructed charge and vertex, but have a poorer mass and momentum resolution. Both the wrong-π^0 events and the right-π^0 events are parametrized in the mass distributions with shapes determined from Monte Carlo; the fraction of wrong π^0's in the peaks are also taken from the Monte Carlo.

The fit of the $D_s^- \to K^{*0}K^-$ mass spectra is a special case due to the presence of the D^- reflection. Following the method described in [16], a simultaneous fit is performed on the two mass spectra obtained from the two possible mass hypotheses (K^- or π^-) for the track associated with the reconstructed K^{*0}. The shapes of the D_s^- and D^- reflections are parametrized with the convolution of a Gaussian and an exponential distribution and determined from Monte Carlo samples, the only free parameters in the fit being the shape parameters of the combinatorial backgrounds, the central values of the Gaussian D_s^- and D^- peaks, and the number of D_s^- and D^- events which are constrained to be the same in the two spectra.

The signal and sideband regions used in this analysis are shown as shaded areas in Fig. 1. The width of the signal regions correspond to $\pm(1.5-2.0)\,\sigma$ depending on the channel, where σ is the Gaussian resolution associated to each D_s^- peak. The sideband regions are chosen to contain mostly combinatorial background. The total number of data candidates in the signal regions is 1620.

4.2 Sample compositions

The reconstruction efficiencies of the D_s^- mesons are determined from fully simulated D_s^- events, separately for the different decay modes and the different sources of D_s^- mesons (B_s^0, B_d^0, B^+, Λ_b, charm and light quark events[2]). The reconstruction efficiency of the $b \to W^- \to D_s^-$ decays is found to be dependent on the fraction of two-body decays of the b hadron. The assumed fraction of two-body decays relies on the CLEO measurement of the fraction of $B_d^0, B^+ \to D_s^{(*)+}\bar{D}^{(*)}$ decays in $B_d^0, B^+ \to D_s^{(*)+}X$ decays, 0.457 ± 0.042 [17], and on an estimate of the fraction of $B_d^0, B^+ \to D_s^{(*)+}\bar{D}^{**}$ decays, 0.2 ± 0.1, derived from [17]. The quoted errors are taken into account when calculating the systematic error due the reconstruction efficiencies. For the direct $b \to D_s^+$ decay the efficiency is found to be much less dependent on the decay channels [18].

[2] Throughout this paper, the generic notation Λ_b is used to designate all b baryons

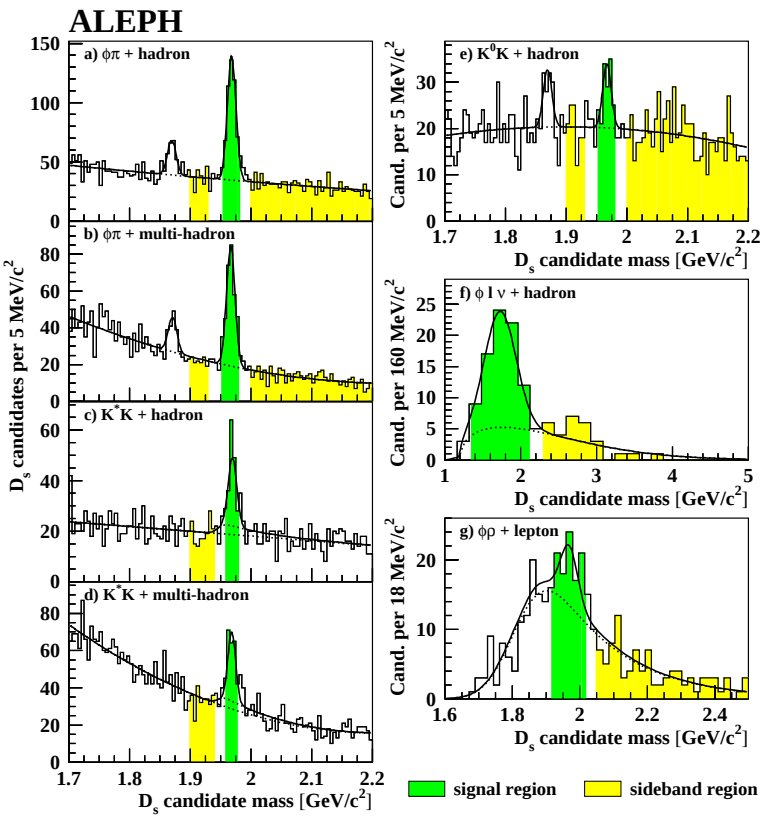

Fig. 1. D_s^- mass spectra for the seven samples. The solid curves show the results of the D_s^- signal fits described in the text, which also take into account true D^- events (**a**, **b**, **e**, **g**) or D^- reflections (**c**, **d**). The dotted curves show the fitted contributions from the combinatorial and D^- reflection backgrounds. The combinatorial background shapes are quadratic polynomials (**a**, **b**, **c**, **d**, **e**), or taken from the Monte Carlo (**f**, **g**). The signal and sideband regions are shaded

Table 3. Values of the physics parameters assumed in this analysis. The quantity $f_{B^+} = \mathcal{B}(\bar{b} \to B^+)$ is taken as $1 - f_{B_d^0} - f_{B_s^0} - f_{\Lambda_b}$. The quoted uncertainties do not include any contribution from $\mathcal{B}(D_s^- \to \phi\pi^-)$. Where several references are quoted, the weighted average is computed, assuming correlated systematic uncertainties between [17] and [24], $\mathcal{B}(B_s^0 \to D_s^- X) = \mathcal{B}(B_s^0 \to D_s^- \ell^+ \nu X)/\mathcal{B}(B_s^0 \to \ell^+ \nu X)$, $\sigma(e^+e^- \to c\bar{c}) = 1232 \pm 104$ pb at $\sqrt{s} = 10.5$ GeV, and $R_c = \mathcal{B}(Z \to c\bar{c})/\mathcal{B}(Z \to q\bar{q}) = 0.172$

Physics parameter	Value and uncertainty	Reference
B^+ lifetime	1.62 ± 0.06 ps	[19]
B_d^0 lifetime	1.56 ± 0.06 ps	[19]
B_s^0 lifetime	1.61 ± 0.10 ps	[19]
Λ_b lifetime	1.14 ± 0.08 ps	[19]
Δm_d	$0.463 \pm 0.018\,\mathrm{ps}^{-1}$	[2]
$R_b = \mathcal{B}(Z \to b\bar{b})/\mathcal{B}(Z \to q\bar{q})$	0.2178 ± 0.0011	[20]
$f_{B_s^0} = \mathcal{B}(\bar{b} \to B_s^0)$	0.112 ± 0.018	[19]
$f_{B_d^0} = \mathcal{B}(\bar{b} \to B_d^0)$	0.378 ± 0.022	[19]
$f_{\Lambda_b} = \mathcal{B}(b \to \Lambda_b)$	0.132 ± 0.041	[19]
$\mathcal{B}(b \to \ell)$	0.1122 ± 0.0021	[20]
$\mathcal{B}(b \to c \to \ell)$	0.0803 ± 0.0034	[20]
$\mathcal{B}(c \to \ell)$	0.098 ± 0.005	[21]
$R_c\,\mathcal{B}(\bar{c} \to D_s^-)\,\mathcal{B}(D_s^- \to \phi\pi^-)$	$(6.27 \pm 0.66) \times 10^{-4}$	[16,22,23]
$R_b\, f_{B_s^0}\,\mathcal{B}(B_s^0 \to D_s^- X)\,\mathcal{B}(D_s^- \to \phi\pi^-)$	$(5.82 \pm 0.83) \times 10^{-4}$	[5,16]
$R_b\, f_{B_s^0}\,\mathcal{B}(B_s^0 \to D_s^- \ell^+ \nu X)\,\mathcal{B}(D_s^- \to \phi\pi^-)$	$(6.53 \pm 0.93) \times 10^{-5}$	[5,16]
$\mathcal{B}(B_d^0, B^+ \to D_s^\pm X)\,\mathcal{B}(D_s^- \to \phi\pi^-)$	$(3.71 \pm 0.28) \times 10^{-3}$	[17,23,24]
$\mathcal{B}(B_d^0, B^+ \to D_s^- X)/\mathcal{B}(B_d^0, B^+ \to D_s^\pm X)$	0.172 ± 0.083	[25]

The list of physics parameters is included in Table 3, together with their values and uncertainties used in this analysis. The values and uncertainties of the D_s^- branching ratios, in particular $\mathcal{B}(D_s^- \to \phi\,\pi^-)$, are irrelevant for this analysis. In the absence of measurements of D_s^- production in Λ_b decays and of D_s^+ production in B_s^0 decays, it is assumed that $\mathcal{B}(\bar{\Lambda}_b \to D_s^+ X) = \mathcal{B}(B_s^0 \to D_s^+ X) = \mathcal{B}(B_d^0, B^+ \to D_s^+ X)$ and $\mathcal{B}(\bar{\Lambda}_b \to D_s^- X) = \mathcal{B}(B_d^0, B^+ \to D_s^- X)$.

The combinatorial background fraction is directly taken from the fit to the D_s^- mass spectrum. In the case of the $D_s^- \to K^{*0}K^-$ and $D_s^- \to \phi\,\rho^-$ decay channels, the fraction of D^- events is also obtained from the mass fits. These events can originate either from charm or b decays. In the $\phi\rho^-$ sample, where an additional lepton is required, no D^-'s are expected from charm. In the other samples, the fraction of D^-'s from b decays is estimated from Monte Carlo studies to be approximately 60%, of which 75% originate from B_d^0 decays. These values are varied within a wide range, but the effect on the result is found to be negligible.

Nine different source fractions are estimated for each sample and displayed in Table 4. In addition, a small fraction of D_s^- mesons produced in the fragmentation of uds events (0.2% on average) is taken into account and added to the fraction of D_s^- mesons produced directly in $c\bar{c}$ events. The quoted uncertainties on the combinatorial background fractions are obtained from the fits to the invariant mass spectra in the data. The uncertainties on the other fractions due to the reconstruction efficiencies (including the Monte Carlo statistical uncertainties and the uncertainties from the fraction of two-body decays in $b \to W^- \to D_s^-$ decays as explained above) are typically less than 0.01. These uncertainties are taken into account, together with those on the physics parameters, in the calculation of systematic errors. On average, the total B_s^0 purity is estimated to be 22%, consisting of 20% of $B_s^0 \to D_s^-$ decays and 2% of $\bar{B}_s^0 \to W^- \to D_s^-$ decays.

5 Proper time determination

5.1 Decay length resolution

The decay length of the B_s^0 candidates is estimated using the algorithms described in Sect. 3. Stringent requirements on the vertex fit probabilities are used to reduce the fraction of B_s^0 candidate vertices containing a misassigned track from the primary vertex. According to Monte Carlo studies, this fraction is 8.5% (21%) for the single hadron (multihadron) vertexing algorithm. The amount of primary vertex background depends on the charged track multiplicity of the final state of the b hadron decay. The probability to assign a primary vertex track to the B_s^0 vertex is reduced for higher multiplicity decays. In a study of the fraction of tracks from the primary vertex, a difference of 7% between data and Monte Carlo has been observed. Including the error from data and Monte Carlo statistics, a total uncertainty of ±9% on the quoted fraction of primary vertex background is taken into account to calculate the contribution to the systematic error.

For events in which at least one track from the B_s^0 decay vertex is correctly associated with the D_s^-, an average resolution on the reconstructed decay length of about 265 μm is observed for both vertex reconstruction algorithms, with a core resolution of ∼160 μm for 50% of the events.

In order to quantitatively determine the difference in the resolution between the Monte Carlo simulation and the data, special samples of D_s^- candidates are selected with relaxed cuts; these samples are enriched in $Z \to b\bar{b}$ events by requiring a displaced vertex in the thrust hemisphere opposite to the D_s^-. In addition the lifetime in the hemisphere of the D_s^- candidate is required to be small. Comparing the negative side of the b hadron lifetime distribution in data and Monte Carlo indicates that the decay length resolution is too good in the Monte Carlo by a factor $S_{MC} = 1.04 \pm 0.03$. To take this observed difference into account, a correction is applied to each proper time resolution function by multiplying the width of the decay-length-dependent part by 1.04. The 3% statistical uncertainty on S_{MC} is propagated as a systematic uncertainty on the final results.

5.2 B_s^0 momentum reconstruction

The momentum of the B_s^0 candidates is estimated using two different algorithms. In both cases, the energy of the B_s^0 candidate is obtained from its estimated momentum assuming the world average B_s^0 mass [19].

For B_s^0 candidates reconstructed as semileptonic decays or reconstructed in events where the missing momentum exceeds 10 GeV/c in the D_s^- hemisphere (estimated as in [26]), the momentum is estimated as the vector sum of the reconstructed D_s^- momentum, the momentum of the track(s) attached to the B_s^0 candidate vertex and the missing momentum in the D_s^- hemisphere. In Monte Carlo studies the average momentum resolution for semileptonic and hadronic decays was found to be 8% and 12% respectively.

For B_s^0 candidates reconstructed as hadronic decays and with low missing momentum in the D_s^- hemisphere, the momentum reconstruction is based on the following algorithm. The momentum sum of the reconstructed D_s^- and the charged tracks associated to the reconstructed B_s^0 vertex are used as an initial estimator of the B_s^0 momentum. All possible combinations of the remaining tracks and neutral particles with momenta greater than 1 GeV/c (assumed to be charged pions or photons) are then added and for each combination the four-momentum is calculated. Using this algorithm on Monte Carlo B_s^0 decays yields a mass distribution with a most probable value of 5.2 GeV/c^2. From this distribution, each combination reconstructed in the data is assigned a probability to be compatible with the B_s^0 hypothesis. The combination with the highest probability is selected and its momentum is used as an estimate of the b hadron momentum. With

Table 4. Composition of the seven samples. The numbers given are the fractions of the D_s^- candidates estimated to be due to the various sources indicated in the first column (after possible B_s^0 and B_d^0 mixing). The last source in the list is the combinatorial background; the D^- contributions are included in the other sources. The numbers of data candidates accepted in the signal regions are given on the header line

	single hadron				multihadron		lepton	all
	$\phi\pi^-$ 539 evts	$K^{*0}K^-$ 178 evts	K^0K^- 158 evts	$\phi\ell^-$ 80 evts	$\phi\pi^-$ 326 evts	$K^{*0}K^-$ 228 evts	$\phi\rho^-$ 111 evts	1620 evts
B_s^0	0.22	0.18	0.11	0.30	0.19	0.15	0.28	0.20
$\bar{B}_s^0$	0.02	0.02	0.01	0.01	0.03	0.02	0.00	0.02
B_d^0	0.01	0.05	0.01	0.02	0.02	0.05	0.00	0.02
$\bar{B}_d^0$	0.08	0.07	0.04	0.04	0.09	0.07	0.01	0.07
B^+	0.01	0.02	0.02	0.04	0.02	0.03	0.00	0.02
B^-	0.08	0.07	0.04	0.04	0.09	0.07	0.01	0.07
$\Lambda_b, \bar{\Lambda}_b$	0.03	0.03	0.01	0.02	0.03	0.03	0.00	0.02
$c\bar{c}$	0.19	0.12	0.04	0.22	0.19	0.11	0.00	0.14
comb.	0.35 ± 0.04	0.45 ± 0.08	0.71 ± 0.08	0.30 ± 0.15	0.33 ± 0.06	0.48 ± 0.09	0.69 ± 0.16	0.43 ± 0.03

this method an average resolution of 9% and an extremely good core resolution of 2% (for 20% of the events) is found.

The uncertainty on the momentum resolution due to the Monte Carlo statistics and to the parametrization used for the dependence of the proper time resolution on the momentum resolution has been estimated to be 7.0%. The performance of the momentum reconstruction has been compared in data and Monte Carlo samples obtained with relaxed cuts. The average reconstructed momentum in the Monte Carlo has been found to be shifted by $0.32\,\mathrm{GeV}/c$; a systematic uncertainty of 1.1% is therefore considered on the momentum estimate. No significant difference in the width of the momentum distributions was observed, and the 1.2% statistical precision of the comparison has been taken as an additional contribution to the uncertainty on the momentum resolution. The total uncertainty on the momentum resolution is 7.1%.

5.3 Proper time resolution

The proper decay time of the B_s^0 candidate is calculated from the reconstructed decay length l and momentum p as

$$t = \frac{l\, m_{B_s^0}}{p}. \qquad (2)$$

The proper time resolution worsens with increasing true decay time t^{true}, as illustrated in Fig. 2. In order to take this dependence into account the distributions of $t - t^{\mathrm{true}}$ are parametrized as functions of t^{true}. The parametrization includes the fraction of primary vertex background.

Resolution functions $r_{jl}(t, t^{\mathrm{true}})$ are determined from Monte Carlo events for each D_s^- source j and for each decay topology l. Four different decay topologies are distinguished based on the vertex reconstruction algorithms (single hadron, multihadron, lepton, $D_s^- \to K^0K^-$). The resolution functions are found to be independent of the D_s^- decay channel (within each topology) and independent of the b hadron species, but separate functions are needed for $\bar{b} \to D_s^-$ and $\bar{b} \to W^+ \to D_s^+$. The resolution

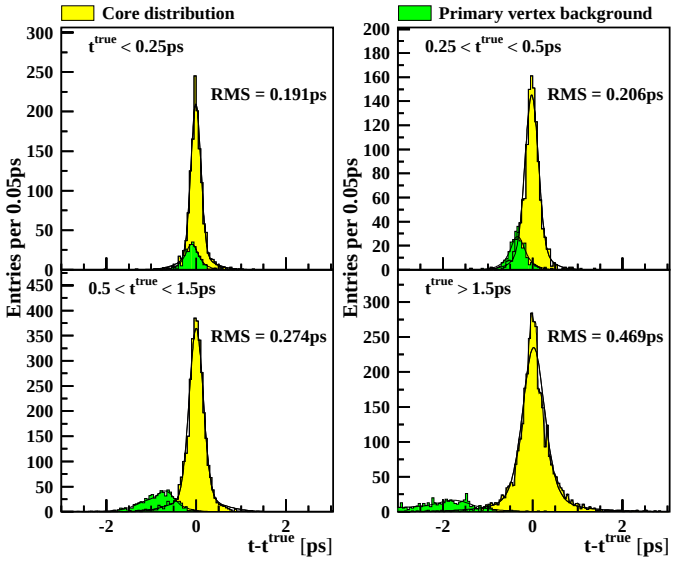

Fig. 2. Proper time resolution for Monte Carlo $D_s^- \to \phi\,\pi^-$ events, reconstructed with the multihadron algorithm, for different true time intervals. Separate distributions are shown for the cases where the number of primary vertex tracks included in the reconstructed B_s^0 vertex is at least one (primary vertex background) or exactly zero (core distributions, for which the RMS values are quoted). The curves represent the integral of the time resolution parametrizations over the corresponding true time intervals

is indeed worse for double charm decays because tracks from the additional charm vertex are sometimes associated with the b hadron vertex.

The resolution function for the b baryon source is assumed to be the same as for $\bar{b} \to W^+ \to D_s^+$, as supported by Monte Carlo studies.

6 Tagging and discrimination

The flavour state of the decaying B_s^0 is estimated from the charge of the reconstructed D_s^-. This final state tag

is incorrect if the D_s^- is produced via a W^-, as in this case the charge of the D_s^- is reversed. The flavour state at production time is estimated using a variety of initial state tags. The power of these tags is enhanced by the means of discriminating variables which have some ability to distinguish whether the tag is correct or not. This approach was used in the ALEPH D_s^--lepton analysis [5] and further details can be found there.

A B_s^0 candidate is "tagged as unmixed (mixed)" when the reconstructed initial and final flavour states are the same (different). By definition, candidates from $c\bar{c}$ or combinatorial backgrounds are only "correctly tagged" if they are "tagged as unmixed".

6.1 Initial state tags

Each B_s^0 candidate event is divided into two hemispheres using the thrust axis to separate the products of the b and the $\bar{b}$ quarks. The hemisphere containing the reconstructed B_s^0 momentum is referred to as the "same hemisphere", and the other one as the "opposite hemisphere". For each B_s^0 candidate, one of the tags described below is used to determine the initial state.

- **Lepton tag:** Muons (electrons) with momentum greater than 3 (2) GeV/c and passing standard lepton identification requirements [15] are searched for in the opposite hemisphere. The sign of the lepton with the highest transverse momentum p_T^ℓ (computed with respect to the axis of the jet containing the lepton candidate) tags the nature of the initial b quark in the opposite hemisphere. This tag is not very efficient due to the low semileptonic branching ratio, but it can have the smallest mistag probability for large values of p_T^ℓ, where backgrounds from $b \to c \to \ell$ and $c \to \ell$ are less important. It takes precedence over the other tags if it is available.
- **Fragmentation kaon tag:** The fragmentation kaon candidate is defined as the highest momentum charged track within 45° of the B_s^0 direction, identified as being more likely to come from the primary vertex than the secondary vertex, and satisfying $\chi_K < 0.5$ and $\chi_K - \chi_\pi > 0.5$. Only tracks which have not already been used to construct the D_s^- or B_s^0 vertices are considered as potential candidates. The sign of the fragmentation kaon candidate tags the sign of the b quark in the same hemisphere. It is used if no opposite hemisphere lepton tag is found.
- **Opposite hemisphere charge tag:** The opposite hemisphere charge is defined as

$$Q_o = \frac{\sum_i^{\text{oppo}} q_i \, |p_\parallel^i|^\kappa}{\sum_i^{\text{oppo}} |p_\parallel^i|^\kappa}, \qquad (3)$$

where the sum is over all charged particles in the opposite hemisphere, $p_\parallel^i$ is the momentum of the i^{th} track projected on the thrust axis, q_i its charge and $\kappa = 0.5$ [27]. The sign of Q_o tags the initial state of the b quark in the opposite hemisphere. This tag is always available but has the largest mistag probability of the three tags. It is used only if no other tag is available.

6.2 Tagging classes and discriminating variables

The B_s^0 candidate events are sorted into five exclusive classes based on the availability and results of the three tags. The definition of the tagging classes and the list of the discriminating variables associated with each class are given in Table 5. The variable Q_s is the sum of the charges of all the tracks in the same hemisphere and carries information on the initial state of the B_s^0. As the sum of charges of tracks originating from the decay of a neutral particle is zero, it is independent of whether the B_s^0 decays as a B_s^0 or a $\bar{B}_s^0$. The variable Z_K is the fraction of the available beam energy taken by the fragmentation kaon candidate (as defined in [5]). It is expected to be large for a true fragmentation kaon which is the first particle produced in the hadronization chain after the B_s^0 [28]. The inclusion of the reconstructed B_s^0 proper time t takes into account that the mistag probability of the fragmentation kaon increases as the B_s^0 vertex approaches the primary vertex, due to the misassignment of tracks between the primary and secondary vertices.

Because the performance of the fragmentation kaon tag depends on the multiplicity of the non-identified B_s^0 decay products, the mistag probabilities and the distributions of the discriminating variables for the correctly and incorrectly tagged events are different (within any given class) for each of the three groups of reconstructed B_s^0 "decay channels", namely $B_s^0 \to D_s^-$+single hadron, $B_s^0 \to D_s^-$+multihadron, and $B_s^0 \to D_s^-$+lepton. However they are independent of the D_s^- decay channel (within a given class and for a given group), since the D_s^- is fully reconstructed.

The signal mistag probability η, as well as the probability distributions for correctly and incorrectly tagged signal events ($r_i(x_i)$ and $w_i(x_i)$) of each discriminating variable x_i, are estimated using large Monte Carlo samples. This is done separately in each tagging class and for each group of channels. The first columns of Table 6 show examples of class populations and mistag rates as determined from Monte Carlo signal events.

The various discriminating variables chosen in each class, $x_1, x_2, \ldots$, are combined into a single effective discriminating variable x^{eff}, according to the prescription developed for the D_s^--lepton analysis [5]. This new variable is defined in each tagging class and for each group of B_s^0 decay channels as

$$x^{\text{eff}} = \frac{\eta \, w_1(x_1) \, w_2(x_2) \cdots}{(1-\eta) \, r_1(x_1) \, r_2(x_2) \cdots + \eta \, w_1(x_1) \, w_2(x_2) \cdots}, \qquad (4)$$

and takes values between 0 and 1. A small value indicates that the initial state of the B_s^0 candidate is likely to have been correctly tagged.

Table 5. The tag and discriminating variables used in each class. The quantities $S(Q_o)$, $S(K)$ and $S(\ell)$ are the signs of the opposite hemisphere charge, the fragmentation kaon and the opposite lepton

Class	Available tags (in addition to $S(Q_o)$)	Tag used	Discriminating variables used					
1		$S(Q_o)$	$Q_s \times S(Q_o)$	$Q_o \times S(Q_o) = \lvert Q_o \rvert$				
2	$S(K)$	$S(K)$	$Q_s \times S(K)$	$Q_o \times S(K)$		Z_K	χ_π	t
3	$S(\ell)$	$S(\ell)$	$Q_s \times S(\ell)$	$Q_o \times S(\ell)$	p_T^ℓ			
4	$S(K) = -S(\ell)$, agree	$S(\ell)$	$Q_s \times S(\ell)$	$Q_o \times S(\ell)$	p_T^ℓ	Z_K	χ_π	t
5	$S(K) = S(\ell)$, disagree	$S(\ell)$	$Q_s \times S(\ell)$	$Q_o \times S(\ell)$	p_T^ℓ	Z_K	χ_π	t

Table 6. The fraction of events, mistag probability η and effective mistag probability η^{eff} in each class as determined from Monte Carlo signal events reconstructed with the single hadron vertexing algorithm. The first uncertainties quoted on the fractions and on η are statistical. The second uncertainties quoted on η are the systematic uncertainties described in Sect. 6.3. The difference between η and η^{eff} reflects the gain in tagging performance obtained from the use of the discriminating variable x^{eff}

Class	Fraction (%)	Mistag η (%)	Effective mistag η^{eff} (%)
1	54.8 ± 0.5	$37.3 \pm 0.6 \pm 0.8$	31 ± 1
2	20.8 ± 0.4	$25.6 \pm 0.9 \pm 2.0$	20 ± 2
3	17.7 ± 0.3	$34.5 \pm 1.0\ ^{+1.8}_{-1.5}$	22 ± 2
4	4.0 ± 0.2	$17.9 \pm 1.6\ ^{+1.6}_{-1.3}$	14 ± 2
5	2.6 ± 0.1	$59.2 \pm 2.7\ ^{+2.2}_{-1.6}$	25 ± 3
ALL	100.0 ± 0.0	34.2 ± 0.4	26 ± 1

The probability density functions $G^c_{jkl}(x^{\text{eff}})$ of x^{eff} are determined for each D_s^- source j in each tagging class k and for each group of B_s^0 decay channels l, separately for the correctly ($c = +1$) and incorrectly ($c = -1$) tagged events. This determination (as well as the estimation of the corresponding mistag probabilities η_{jkl}) is based on Monte Carlo events, except for the combinatorial background where the data sidebands are used. The functions $G^c_{jkl}(x^{\text{eff}})$ are found to be similar, and therefore assumed to be equal, for all b hadron species. Examples of these distributions are shown in Fig. 3.

The enhancement of the tagging power provided by the variable x^{eff} depends on the difference between the $G^+_{jkl}(x^{\text{eff}})$ and $G^-_{jkl}(x^{\text{eff}})$ distributions, and can be quantified in terms of effective mistag rates, as described in [5]. Some effective mistag rates for the B_s^0 signal are given in Table 6.

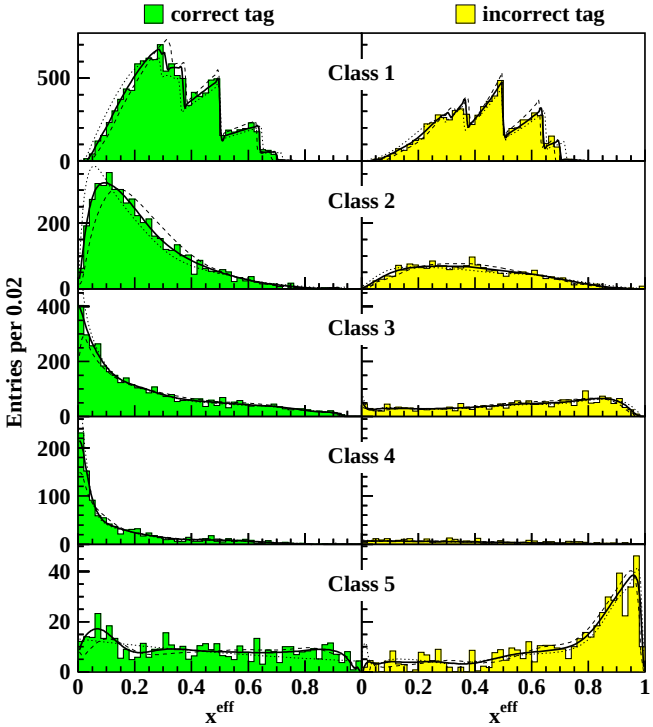

Fig. 3. Distributions of the effective discriminating variable x^{eff}, as determined in each tagging class from correctly tagged and incorrectly tagged b hadron Monte Carlo events reconstructed with the single hadron vertexing algorithm. The discontinuities observed in Class 1 are due to the discrete nature of Q_s. The plain curves are the parametrizations of these distributions, which are proportional to the probability density functions $G^c_{jkl}(x^{\text{eff}})$ used in the likelihood function. The dashed and dotted curves show modified parametrizations used for systematic studies

6.3 Systematic studies on tagging

As a check of the accuracy of the simulation with respect to the mistag probabilities and the distributions of the discriminating variables, a comparison between the data and Monte Carlo distributions is performed, and observed differences are propagated as systematic uncertainties. This is done by constructing a "best case" and a "worst case" scenario in which the set of nominal mistags η_{jkl} and distributions G^c_{jkl} are replaced by an alternative set of mistags and distributions which have been appropriately modified to yield a better or worse tagging performance.

Following the method used in the D_s^--lepton analysis [5], the modified distributions, $G^{c\,\text{best}}_{jkl}$ and $G^{c\,\text{worst}}_{jkl}$, are taken as the Monte Carlo distributions of modified effective discriminating variables $x^{\text{eff best}}$ and $x^{\text{eff worst}}$ defined,

Table 7. The offsets and scale factors, with their statistical uncertainties, representing the difference between Monte Carlo and data for some of the discriminating variables (the values for χ_π and Z_K are from [5])

Variable	Offset	Scale factor
Q_o	-0.0005 ± 0.0024	1.026 ± 0.011
Q_s	$+0.023 \pm 0.019$	1.025 ± 0.009
χ_π	-0.025 ± 0.024	1.01 ± 0.02
Z_K	$+0.001 \pm 0.001$	0.95 ± 0.02

in analogy with (4), as

$$x^{\text{eff best}} = \frac{\eta^{\text{best}}\, w_1^{\text{best}}(x_1)\, w_2^{\text{best}}(x_2) \cdots}{(1-\eta^{\text{best}})\, r_1^{\text{best}}(x_1)\, r_2^{\text{best}}(x_2) \cdots + \eta^{\text{best}}\, w_1^{\text{best}}(x_1)\, w_2^{\text{best}}(x_2) \cdots}\,, \quad (5)$$

and similarly for $x^{\text{eff worst}}$, using modified signal mistags η^{best} and η^{worst}, as well as modified discriminating variable distributions (w^{best}, w^{worst}, r^{best} and r^{worst}). This procedure of varying, in a coherent way, all the quantities relevant to a particular tag tends to overestimate the systematic effects, and is thus rather conservative. Examples of $G_{jkl}^{c\,\text{best}}$ and $G_{jkl}^{c\,\text{worst}}$ functions used in this analysis are shown as dotted and dashed curves in Fig. 3. All background mistag biases considered to construct the worst and best cases are taken to be equal to those assumed for the signal.

The modified distributions for variables Q_o, Q_s, χ_π, and Z_K are obtained by applying offsets and scale factors to the nominal Monte Carlo distributions, as in the D_s^--lepton analysis. These offsets and scale factors, shown in Table 7, are estimated from a comparison between Monte Carlo and data distributions obtained with relaxed selection cuts. These changes are also propagated to the Q_o mistag in Class 1 and yield modified mistags η^{best} and η^{worst} which differ from their nominal values by approximately $\pm 0.8\%$ (absolute). For the fragmentation kaon tag, an absolute mistag bias of $\pm 2\%$ is considered.

The mistag of the opposite lepton tag and the power of p_T^ℓ as a discriminating variable is determined by the fraction of leptons originating directly from a b decay, i.e., by the branching ratios $\mathcal{B}(b \to \ell)$, $\mathcal{B}(b \to c \to \ell)$ and $\mathcal{B}(c \to \ell)$ given in Table 3. To a lesser extent it is also influenced by the assumed model for the decay process and systematics in the lepton identification purity and efficiency. For the best (worst) case, the assumed value of $\mathcal{B}(b \to \ell)$ is increased (decreased) by its uncertainty, the other branching ratios moved in the opposite direction, and the assumed decay model is modified so as to give a better (poorer) tagging performance. The modified mistags for Classes 3, 4 and 5, and all the modified r and w distributions involving p_T^ℓ are determined in the same way as the corresponding nominal quantities, but from Monte Carlo events reweighted to the desired branching ratios and decay model. Absolute changes of 1–2% are obtained on the mistags (see Table 6 for details).

7 Likelihood function

Each b hadron source has a different probability distribution function for the true proper time t^{true} and for the discrete variable λ, defined to take the value -1 for the mixed case or $+1$ for the unmixed case. Assuming CP conservation and equal lifetime for the two CP eigenstates in each neutral b meson system, the joint probability distribution of t^{true} and λ can be written as

$$p_j(\lambda, t^{\text{true}}) = \frac{e^{-t^{\text{true}}/\tau_j}}{2\tau_j}\, \left[1 + \lambda \cos\left(\Delta m_j\, t^{\text{true}}\right)\right]\,, \quad (6)$$

where τ_j and Δm_j are the lifetime and oscillation frequency of b hadron source j (with the convention that $\Delta m_j = 0$ for B^+ and Λ_b sources). The joint probability distribution of the reconstructed proper time t and of λ is obtained as the convolution of $p_j(\lambda, t^{\text{true}})$ with the resolution function $r_{jl}(t, t^{\text{true}})$ for the appropriate source j and sample l (see Sect. 5.3):

$$h_{jl}(\lambda, t) = \int_0^\infty r_{jl}(t, t^{\text{true}})\, p_j(\lambda, t^{\text{true}})\, dt^{\text{true}} \quad (7)$$

For all other sources (i.e., $c\bar{c}$ and combinatorial background), $h_{jl}(-1, t) = 0$ since these sources are unmixed by definition, and $h_{jl}(+1, t)$ are just the reconstructed proper time distributions. For $c\bar{c}$ background, these distributions are determined from Monte Carlo samples; they are consistent with the resolution function for zero-lifetime events and are parametrized with the sum of two Gaussian functions. The reconstructed proper time distributions of the combinatorial background are determined from the data events in the D_s^- sidebands, separately for the tagged-as-mixed and tagged-as-unmixed candidates. They are found to be independent of the tagging result within the available statistics. These functions are parametrized as the sum of two Gaussian functions centred at zero and the convolution of an exponential function with a Gaussian function. The exponential term is used to describe the significant tails observed at positive proper times; these tails are due to the inclusion of b hadron decay products in the combinatorial D_s^- candidates.

The likelihood function used in this analysis is based on the values taken by three different variables in the selected data events. These variables are the reconstructed proper time t, the tagging result μ, taking the value -1 for events tagged as mixed or $+1$ for those tagged as unmixed, and the effective discriminating variable x^{eff}. The use of the discriminating variable x^{eff} in this likelihood function is reduced to the use of two sets of functions of x^{eff}, $X_{jkl}(x^{\text{eff}})$ and $Y_{jkl}(x^{\text{eff}})$, whose values can be interpreted as event-by-event mistag probabilities and fractions of the different D_s^- sources respectively. The likelihood of the total sample is written as

$$\mathcal{L} = C \prod_{l}^{7\,\text{samples}} \prod_{k}^{5\,\text{classes}} \prod_{i}^{N_{kl}\,\text{events}} f_{kl}(x_{ikl}^{\text{eff}}, \mu_{ikl}, t_{ikl})\,, \quad (8)$$

where C is a constant independent of b oscillation frequencies and lifetimes, N_{kl} is the number of selected candidates

from sample l falling in tagging class k, and where

$$f_{kl}(x^{\rm eff},\mu,t) = \sum_{j}^{9\ \text{sources}} Y_{jkl}(x^{\rm eff})\left[\left(1-X_{jkl}(x^{\rm eff})\right)h_{jl}(\mu\epsilon_j,t) + X_{jkl}(x^{\rm eff})h_{jl}(-\mu\epsilon_j,t)\right].$$

The quantity ϵ_j is equal to -1 if the D_s^- is produced via a virtual W^- in source j, or $+1$ otherwise; it multiplies μ in order to reverse the tag result for sources where the initial state tag provided by the D_s^- charge is wrong.

The event-by-event quantities $X_{jkl}(x^{\rm eff})$ and $Y_{jkl}(x^{\rm eff})$ are computed from the distributions $G^c_{jkl}(x^{\rm eff})$ and mistag probabilities η_{jkl} introduced in Sect. 6.2,

$$X_{jkl}(x^{\rm eff}) = \eta_{jkl}\,\frac{G^-_{jkl}(x^{\rm eff})}{G_{jkl}(x^{\rm eff})}\,,$$
$$Y_{jkl}(x^{\rm eff}) = \alpha_{jkl}\,\frac{G_{jkl}(x^{\rm eff})}{\sum_{j'}\alpha_{j'kl}G_{j'kl}(x^{\rm eff})}\,, \qquad (10)$$

where $G_{jkl}(x^{\rm eff}) = (1-\eta_{jkl})G^+_{jkl}(x^{\rm eff})+\eta_{jkl}G^-_{jkl}(x^{\rm eff})$ and where α_{jkl} are the source fractions, satisfying $\sum_j \alpha_{jkl} = 1$.

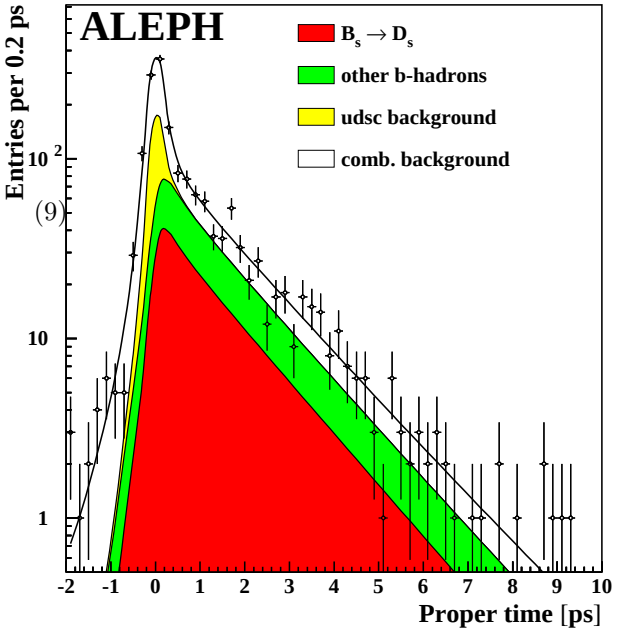

Fig. 4. Distribution of the measured proper time in the data. The curves show the result of the lifetime fit and the contributions of the different components to the sample

8 B_s^0 lifetime measurement

The B_s^0 lifetime τ_s is a parameter of the likelihood function and can therefore be determined by minimizing the corresponding negative log-likelihood. However, for the purpose of this lifetime measurement for which the tagging information is not important, anything related to the mistag probability and the discriminating variable $x^{\rm eff}$ is removed from the likelihood function. This is done by setting, in the probability density function of (9), $X_{jkl}(x^{\rm eff})$ to 1/2 and $Y_{jkl}(x^{\rm eff})$ to the fraction of source j in sample l averaged over all tagging classes k.

Maximizing the modified likelihood with respect to the B_s^0 lifetime yields $\tau_s = 1.47 \pm 0.14$ ps. This measurement is consistent, within the quoted statistical uncertainty, with the world average of 1.61 ± 0.10 ps [19]. The proper time distribution of the data sample is shown in Fig. 4, together with the result of the fit.

The various systematic effects are related to underlying parameters which are held fixed in the lifetime fit. Their corresponding contributions to the systematic uncertainty on the B_s^0 lifetime are estimated by changing in turn the values of the fixed parameters by $\pm 1\sigma$, where σ is the uncertainty on the parameters (given in Table 3 for the physics parameters). The different sources of systematic effects can be divided into the following categories:

- **Combinatorial background:** the fraction of combinatorial background is changed, independently for each of the seven samples, by the uncertainty estimated from the fit to the D_s^- mass spectrum in the data. In addition, the shape of the proper time distribution for the combinatorial background is varied within the uncertainty of the parametrization.
- **Reconstruction efficiencies:** the estimated reconstruction efficiencies are changed by their uncertainties; this is done independently for each of the five D_s^- decay modes and separately for the $\bar{b} \to D_s^-$ efficiencies, the $b \to D_s^-$ efficiencies, and the $\bar{c} \to D_s^-$ efficiencies.
- **Proper time resolution and bias:** various parameters of the proper time resolution functions are varied, as described in Sect. 5, including the fraction of primary vertex background, the decay length resolution, the momentum resolution and bias.
- **Analysis bias:** to check for possible biases in the event selection and in the convolution procedure, the analysis is performed on a Monte Carlo sample of pure B_s^0 decays generated with an input lifetime of 1.5 ps. The fitted lifetime is $\tau_s = 1.512 \pm 0.020$ ps, consistent with the input value. The statistical uncertainty of this result is taken as an upper limit on any possible bias.
- **Fragmentation in b decays:** the selection efficiencies estimated from the Monte Carlo are sensitive to the momentum distribution of the b hadrons. The average fraction of the beam energy taken by the b hadron in the Monte Carlo is $x_E(\text{MC}) = 0.714 \pm 0.004$; the same quantity measured in the data is $x_E(\text{ALEPH}) = 0.715 \pm 0.015$ [30]. Using new efficiencies obtained by rescaling the momenta of the b hadrons in the Monte Carlo by the statistical uncertainty measured in the data leads to a variation in the fitted B_s^0 lifetime of ∓ 0.028 ps [18].
- **Other b hadron lifetimes:** the B_d^0, B^+ and Λ_b lifetimes are varied independently.
- **Difference in decay width:** possible decay width differences, $\Delta\Gamma_s/\Gamma_s$ and $\Delta\Gamma_d/\Gamma_d$, between the two mass

Table 8. Contributions to the systematic uncertainty on the B_s^0 lifetime measurement. The contributions associated with a physics parameter are given for the parameter variations shown in Table 3 or in Section 8 with the appropriate sign correlation ($\pm$ or $\mp$). The contributions from $\mathcal{B}(b \to c \to \ell)$ and $\mathcal{B}(B_d^0, B^+ \to D_s^- X)/\mathcal{B}(B_d^0, B^+ \to D_s^\pm X)$ are smaller than 0.0005 ps

Source of systematics	$\Delta\tau_s$ [ps]	Source of systematics	$\Delta\tau_s$ [ps]
Comb. background fraction	$^{+0.018}_{-0.013}$	$\Delta\Gamma_s/\Gamma_s$	$^{-0.024}_{+0.000}$
Comb. background shape	0.036	R_b	∓ 0.001
Reconstruction efficiencies	0.008	$f_{B_s^0}$	± 0.004
Proper time resolution	0.019	$f_{B_d^0}$	± 0.001
Momentum bias	0.016	f_{Λ_b}	± 0.015
Analysis bias	0.020	$R_c\,\mathcal{B}(\bar{c} \to D_s^-)$	± 0.026
b fragmentation	∓ 0.028	$R_b\, f_{B_s^0}\,\mathcal{B}(B_s^0 \to D_s^- X)$	∓ 0.010
B^+ lifetime	∓ 0.020	$R_b\, f_{B_s^0}\,\mathcal{B}(B_s^0 \to D_s^- \ell^+ \nu X)$	∓ 0.001
B_d^0 lifetime	∓ 0.021	$\mathcal{B}(B_d^0, B^+ \to D_s^\pm X)$	∓ 0.013
Λ_b lifetime	∓ 0.007	Quadratic sum of all contributions	0.076

eigenstates of the B_s^0 meson and the two mass eigenstates of the B_d^0 meson have been neglected in the likelihood fit. While $\Delta\Gamma_d/\Gamma_d$ is predicted to be less than 1%, $\Delta\Gamma_s/\Gamma_s$ could indeed be significant enough to bias the results. The measurement is therefore repeated with a modified likelihood assuming a fixed value of $\Delta\Gamma_s/\Gamma_s = 0.27$, equal to the theoretical prediction of [29], $\Delta\Gamma_s/\Gamma_s = 0.16^{+0.11}_{-0.09}$, plus its quoted positive uncertainty. The resulting lifetime measurement is reduced by 0.024 ps compared to the nominal measurement obtained with $\Delta\Gamma_s/\Gamma_s = 0$. This shift is taken as a systematic uncertainty.

– **Branching ratios:** the products $R_b\, f_{B_s^0}\mathcal{B}(B_s^0 \to D_s^- X)$, $R_b f_{B_s^0}\mathcal{B}(B_s^0 \to D_s^- \ell^+ \nu X)$ and $R_c\mathcal{B}(\to \bar{c})D_s^-$ are varied independently; the quantities used to compute the backgrounds from $b \to W^- \to D_s^-$ decays or from direct decays of non-B_s^0 b-hadrons, i.e., R_b, $f_{B_s^0}$, $f_{B_d^0}$, f_{Λ_b}, $\mathcal{B}(B_d^0 \to D_s^\pm X)$, $\mathcal{B}(B_d^0, B^+ \to D_s^- X)/\,\mathcal{B}(B_d^0, B^+ \to D_s^\pm X)$ and $\mathcal{B}(b \to c \to \ell)$, are varied separately.

All the contributions, shown by category in Table 8, are added in quadrature to give a total systematic uncertainty of ± 0.08 ps.

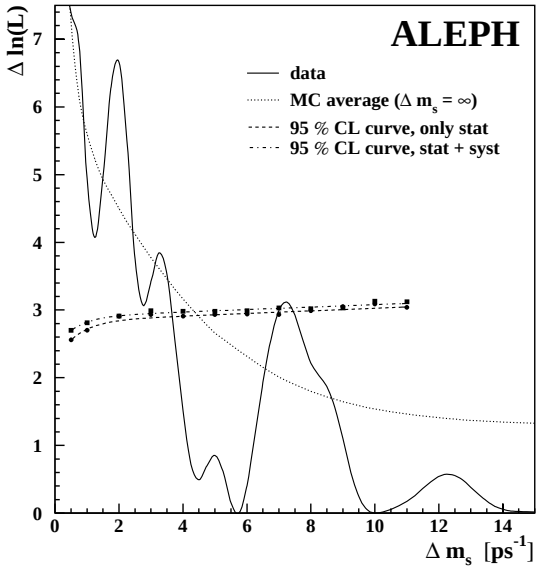

Fig. 5. Negative log-likelihood difference with respect to the minimum as a function of Δm_s. The solid curve shows the data. The dotted curve shows the fast Monte Carlo expectation for $\Delta m_s^{\text{true}} = \infty$. The dot-dashed (dashed) curve is the 95% CL curve with (without) systematic effects included

9 B_s^0 oscillation results

Several published experimental results on B_s^0 mixing [4, 5, 8] were obtained using a method where the log-likelihood difference with respect to the minimum of $-\ln\mathcal{L}$ is calibrated with fast Monte Carlo samples to get the correct confidence level for excluding Δm_s values. For comparison, the results of this analysis are first presented using the same likelihood method. However, the final results are obtained here with a new method [31] inspired from Fourier analysis, called the "amplitude method", which is more sensitive and has the advantage of allowing the outcome of different analyses to be easily combined.

9.1 Results with the likelihood method

The negative log-likelihood difference with respect to the minimum is shown in Fig. 5 for the total data sample. Minima occur at $\Delta m_s = 5.7$, 10.0 and 15.5 ps^{-1}, but none of them is significant enough to claim a measurement.

In order to exclude values of Δm_s, 95% CL curves (shown also in Fig. 5) are determined from a large number of statistically independent fast Monte Carlo experiments generated at different true values of Δm_s, with the same number of events in each sample and each tagging class as observed in the data. The fast Monte Carlo generator takes into account all the details on the sample compositions, the resolution functions, the mistag rates, and the distributions of x^{eff}. Systematic effects are incorporated

by varying (from one experiment to another) all the parameters used in the generation within their estimated uncertainties. Using this fast Monte Carlo calibration, the data exclude (at 95% CL) all values of Δm_s smaller than $3.7\,\mathrm{ps}^{-1}$ and in the range 7.0–$7.4\,\mathrm{ps}^{-1}$.

A check has been made on fully simulated Monte Carlo signal events that there is no bias, within the statistical uncertainty, when fitting for Δm_s.

9.2 Amplitude method and sensitivity of the analysis

Rather than looking for an oscillation in the proper time spectrum of the data sample, one can look for a peak in a frequency spectrum. Following the method of [31], the magnitude of B_s^0 proper time oscillations is measured at fixed values of the frequency Δm_s, using a modified likelihood function that depends on a new parameter, the oscillation amplitude $\mathcal{A}$. For the present analysis, the required modification is to replace the probability density function of the B_s^0 and $\bar{B}_s^0$ sources given in (6) with

$$\frac{e^{-t^{\mathrm{true}}/\tau_s}}{2\tau_s}\left[1+\lambda\mathcal{A}\cos\left(\Delta m_s\, t^{\mathrm{true}}\right)\right]. \qquad (11)$$

For each value of Δm_s, the new negative log-likelihood is minimized with respect to $\mathcal{A}$, leaving all other parameters (including Δm_s) fixed. The minimum is well behaved and very close to parabolic. At each value of Δm_s one can thus obtain a measurement of the amplitude with Gaussian error, $\mathcal{A}\pm\sigma_{\mathcal{A}}^{\mathrm{stat}}$. Each systematic effect considered in the analysis is propagated to an additional uncertainty on the measured amplitudes using the prescription given in [31].

If $\Delta m_s = \Delta m_s^{\mathrm{true}}$, one expects $\mathcal{A}=1$ within the total uncertainty $\sigma_{\mathcal{A}}$; however, if Δm_s is far from its true value, a measurement consistent with $\mathcal{A}=0$ is expected. A value of Δm_s can be excluded at 95% CL if $\mathcal{A}+\xi\sigma_{\mathcal{A}}\leq 1$, where $\xi=1.645$ satisfies $\int_{-\infty}^{\xi}\frac{1}{\sqrt{2\pi}}e^{-\frac{1}{2}x^2}dx = 95\%$. The lower limit on Δm_s is defined as the highest value below which all values of Δm_s are excluded at the specified confidence level. If the true value of Δm_s is very high, one expects $\mathcal{A}=0$, and all values of Δm_s such that $\xi\sigma_{\mathcal{A}}(\Delta m_s)<1$ are expected to be excluded at 95% CL. Because of the proper time resolution, the quantity $\sigma_{\mathcal{A}}(\Delta m_s)$ is an increasing function of Δm_s (high frequencies are more difficult to observe), and one therefore expects to be able to exclude individual Δm_s values up to $\Delta m_s^{\mathrm{sens}}$ where $\Delta m_s^{\mathrm{sens}}$, called here the sensitivity of the analysis, is defined by $\xi\sigma_{\mathcal{A}}(\Delta m_s^{\mathrm{sens}})=1$.

The consistency between the fast Monte Carlo generation and the expectations $\mathcal{A}=0$ and $\mathcal{A}=1$ for the fitted amplitude has been checked. The average amplitude over many fast Monte Carlo experiments is indeed found to be consistent with unity for $\Delta m_s=\Delta m_s^{\mathrm{true}}$ and with zero for any value of Δm_s if $\Delta m_s^{\mathrm{true}}=\infty$.

The estimate $\sigma_{\mathcal{A}}^{\mathrm{stat}}$ of the statistical uncertainty on the amplitude can be checked by studying the distribution of $\mathcal{A}/\sigma_{\mathcal{A}}^{\mathrm{stat}}$ for cases where $\mathcal{A}=0$ is expected. The mean value and RMS of such a distribution obtained with fast Monte Carlo experiments generated with $\Delta m_s^{\mathrm{true}}=\infty$ are found to be consistent with 0 and 1.

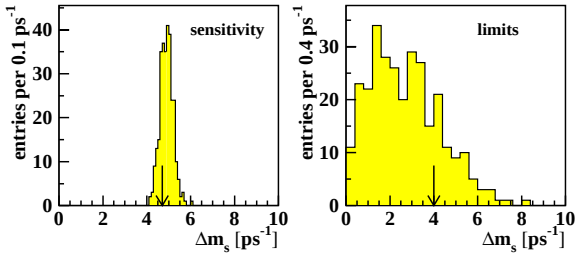

Fig. 6. Distributions of the sensitivity and the 95% CL lower limit on Δm_s obtained with the amplitude method in 300 fast Monte Carlo experiments generated without systematics at $\Delta m_s^{\mathrm{true}}=\infty$. The mean values are 4.9 and $2.7\,\mathrm{ps}^{-1}$ respectively. The arrows indicate the values obtained in the data (statistical uncertainties only)

The sensitivity (without the inclusion of systematic uncertainties) is derived from each fast Monte Carlo experiment generated with $\Delta m_s^{\mathrm{true}}=\infty$; its distribution, shown in Fig. 6, has a mean value of $4.9\,\mathrm{ps}^{-1}$ and an RMS spread of $0.3\,\mathrm{ps}^{-1}$. The distribution of the lower limits set in the same experiments, also shown in Fig. 6, is broad and has a median value of $2.5\,\mathrm{ps}^{-1}$.

9.3 Results with the amplitude method

The systematic uncertainty on the B_s^0 oscillation amplitude $\mathcal{A}$ is estimated using a similar procedure as for the B_s^0 lifetime measurement, described in Sect. 8. This includes also the variation of the B_s^0 lifetime and the B_d^0 oscillation frequency. In contrast to the B_s^0 lifetime analysis, varying the b hadron lifetimes and the parametrizations of the proper time distributions of the combinatorial background within their uncertainties has very little effect.

Additional systematic uncertainties due to the tagging and discrimination are estimated by implementing the best case and worst case scenarios, described in Sect. 6.3; in addition, all the class mistag probabilities are varied by their Monte Carlo statistical uncertainties, independently in each tagging class.

The amplitude results are summarized in Table 9 and displayed in Fig. 7a as a function of Δm_s. As for the likelihood method, no significant oscillation signal can be claimed. All values of Δm_s below $3.9\,\mathrm{ps}^{-1}$, and between 6.5 and $8.8\,\mathrm{ps}^{-1}$, are excluded at 95% CL. The sensitivity, estimated from the data, is $4.1\,\mathrm{ps}^{-1}$.

Without the systematic uncertainties, the lower limit and sensitivity from the data would be 4.0 and $4.7\,\mathrm{ps}^{-1}$, respectively. If one assumes that $\Delta m_s^{\mathrm{true}}$ is very large, these results can be compared with the fast Monte Carlo distributions of Fig. 6. The lower limit from the data is higher than the expectation, but still quite probable since 22% of fast Monte Carlo experiments give a limit above the one set in the data. The sensitivity estimated from the data is within one standard deviation of the Monte Carlo expectation.

Table 9. Measurements of the B_s^0 oscillation amplitude $\mathcal{A}$ obtained in this analysis at different values of Δm_s, together with the statistical uncertainty $\sigma_{\mathcal{A}}^{\rm stat}$ and the total systematic uncertainty $\sigma_{\mathcal{A}}^{\rm syst}$; a breakdown of $\sigma_{\mathcal{A}}^{\rm syst}$ in several categories of systematic effects is also given

Δm_s [ps^{-1}]	0.00	2.00	4.00	6.00	8.00	10.00
$\mathcal{A}$	-0.03	-0.52	$+0.13$	$+0.46$	-1.31	$+1.22$
$\sigma_{\mathcal{A}}^{\rm stat}$	±0.24	±0.41	±0.56	±0.70	±0.99	±1.50
$\sigma_{\mathcal{A}}^{\rm syst}$	$\pm^{0.23}_{0.35}$	±0.17	$\pm^{0.22}_{0.33}$	±0.29	±0.25	$\pm^{0.46}_{0.72}$
Systematic contributions:						
– combinatorial background	±0.01	±0.01	$\pm^{0.12}_{0.08}$	$\pm^{0.18}_{0.12}$	$\pm^{0.11}_{0.06}$	$\pm^{0.11}_{0.27}$
– reconstruction efficiencies	$\pm^{0.11}_{0.30}$	$\pm^{0.05}_{0.12}$	$\pm^{0.10}_{0.24}$	$\pm^{0.05}_{0.22}$	±0.19	$\pm^{0.30}_{0.62}$
– time resolution and bias	±0.00	±0.01	±0.04	±0.08	±0.04	±0.05
– tagging and discrimination	±0.04	$\pm^{0.12}_{0.07}$	$\pm^{0.08}_{0.18}$	$\pm^{0.20}_{0.06}$	$\pm^{0.05}_{0.12}$	$\pm^{0.21}_{0.12}$
– b-fragmentation	±0.02	±0.04	±0.04	±0.04	±0.05	$\pm^{0.10}_{0.09}$
– b-lifetimes, Δm_d, $\Delta\Gamma_s/\Gamma_s$	±0.01	±0.00	±0.02	±0.02	±0.03	±0.06
– branching ratios (signal)	$\pm^{0.14}_{0.11}$	$\pm^{0.09}_{0.07}$	$\pm^{0.09}_{0.07}$	±0.01	$\pm^{0.07}_{0.06}$	$\pm^{0.21}_{0.16}$
– branching ratios (background)	±0.12	±0.04	±0.04	±0.04	±0.04	±0.09

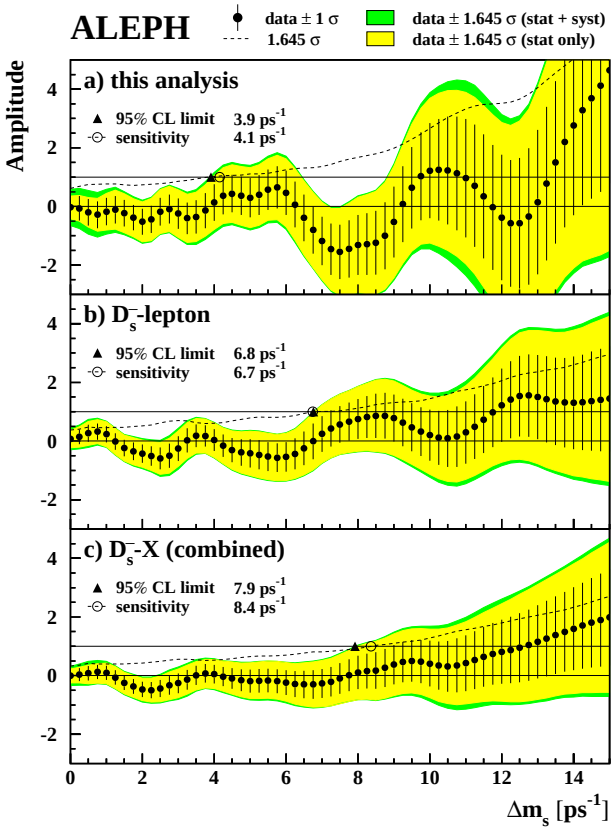

Fig. 7. Measured amplitude as a function of Δm_s for **a**) this analysis, **b**) the D_s^--lepton analysis [5] and **c**) the combination of the two analyses. The error bars represent the 1σ total uncertainties, and the shaded bands show the one-sided 95% CL contour, with and without systematic effects included

As a check, a straight line fit of the amplitude plot in the data (Fig. 7a) is performed, taking into account the statistical correlations between the measurements at different values of Δm_s which are modelled with a simple Breit-Wigner function with width $\Gamma_s = 1/\tau_s$ [31]. The average amplitude, in the range $0 \le \Delta m_s \le 15\,\text{ps}^{-1}$, is found to be -0.11 ± 0.18, consistent with zero within the quoted statistical uncertainty, as expected for no significant signal.

10 Combination with D_s^--lepton results

The ALEPH D_s^--lepton analysis [5] yields $\tau_s = 1.54^{+0.14}_{-0.13}\,(\text{stat}) \pm 0.04(\text{syst})$ ps and, using the likelihood method referred to the minimum, $\Delta m_s > 6.6\,\text{ps}^{-1}$ at 95% CL. The same analysis is repeated using the amplitude method. The resulting amplitude plot is shown in Fig. 7b, from which all values of Δm_s below $6.8\,\text{ps}^{-1}$ are excluded at 95% CL. The systematic uncertainty on the amplitude measurements is small, as can be seen from Table 10.

At each value of Δm_s the B_s^0 oscillation amplitudes measured in the two analyses can be combined using a standard averaging procedure. The following sources of systematic uncertainty are common and therefore treated as fully correlated: the values assumed for $f_{B_s^0}$, $f_{B_d^0}$, Δm_d and the various b hadron lifetimes, the decay length resolution bias in the Monte Carlo simulation $S_{\rm MC}$, the mistag probabilities, and the use of the effective discriminating variable. Since the physics parameters assumed in the two analyses are slightly different, the D_s^--lepton results are adjusted to the more recent set of physics parameters listed in Table 3 before averaging. The combined amplitude results are listed in Table 11 and displayed in Fig. 7c. No B_s^0 oscillation signal is seen and all values of Δm_s below $7.9\,\text{ps}^{-1}$ are excluded at 95% CL. The combined sensitivity is $8.4\,\text{ps}^{-1}$.

Combining the B_s^0 lifetime results of the two analyses yields $\tau_s = 1.51 \pm 0.11$ ps.

Table 10. Measurements of the B_s^0 oscillation amplitude $\mathcal{A}$ obtained in the D_s^--lepton analysis [5] at different values of Δm_s, together with the statistical uncertainty $\sigma_{\mathcal{A}}^{\rm stat}$ and the total systematic uncertainty $\sigma_{\mathcal{A}}^{\rm syst}$; a breakdown of $\sigma_{\mathcal{A}}^{\rm syst}$ in several categories of systematic effects is also given

Δm_s [ps^{-1}]	0.00	2.00	4.00	6.00	8.00	10.00
$\mathcal{A}$	$+0.07$	-0.43	$+0.03$	-0.54	$+0.75$	$+0.20$
$\sigma_{\mathcal{A}}^{\rm stat}$	±0.18	±0.28	±0.36	±0.49	±0.67	±0.81
$\sigma_{\mathcal{A}}^{\rm syst}$	$\pm^{0.11}_{0.16}$	$\pm^{0.11}_{0.16}$	$\pm^{0.05}_{0.12}$	±0.11	$\pm^{0.07}_{0.14}$	$\pm^{0.38}_{0.27}$
Systematic contributions:						
– combinatorial background	±0.01	±0.02	$\pm^{0.00}_{0.03}$	$\pm^{0.00}_{0.03}$	$\pm^{0.00}_{0.03}$	±0.01
– time resolution and bias	$\pm^{0.02}_{0.00}$	$\pm^{0.01}_{0.03}$	$\pm^{0.04}_{0.08}$	$\pm^{0.08}_{0.09}$	$\pm^{0.05}_{0.10}$	$\pm^{0.13}_{0.15}$
– tagging and discrimination	$\pm^{0.11}_{0.10}$	$\pm^{0.11}_{0.15}$	$\pm^{0.03}_{0.08}$	$\pm^{0.07}_{0.03}$	$\pm^{0.04}_{0.09}$	$\pm^{0.36}_{0.22}$
– b-lifetimes, Δm_d	$\pm^{0.01}_{0.00}$	±0.00	±0.01	±0.01	±0.02	$\pm^{0.00}_{0.01}$
– b-hadron fractions	$\pm^{0.01}_{0.12}$	$\pm^{0.00}_{0.04}$	$\pm^{0.00}_{0.03}$	$\pm^{0.00}_{0.03}$	$\pm^{0.00}_{0.03}$	$\pm^{0.00}_{0.02}$

Table 11. Combined measurements of the B_s^0 oscillation amplitude $\mathcal{A}$ as a function of Δm_s (in ps^{-1}), together with the statistical uncertainty $\sigma_{\mathcal{A}}^{\rm stat}$ and the total systematic uncertainty $\sigma_{\mathcal{A}}^{\rm syst}$. Measurements at two neighbouring values of Δm_s are strongly correlated

Δm_s	$\mathcal{A} \pm\sigma_{\mathcal{A}}^{\rm stat} \pm\sigma_{\mathcal{A}}^{\rm syst}$	Δm_s	$\mathcal{A} \pm\sigma_{\mathcal{A}}^{\rm stat} \pm\sigma_{\mathcal{A}}^{\rm syst}$	Δm_s	$\mathcal{A} \pm\sigma_{\mathcal{A}}^{\rm stat} \pm\sigma_{\mathcal{A}}^{\rm syst}$
0.00	$-0.01 \pm 0.14 \pm 0.14$	5.00	$-0.19 \pm 0.37 \pm 0.14$	10.00	$+0.41 \pm 0.71 \pm 0.31$
0.25	$+0.03 \pm 0.16 \pm 0.14$	5.25	$-0.18 \pm 0.38 \pm 0.14$	10.25	$+0.34 \pm 0.75 \pm 0.35$
0.50	$+0.08 \pm 0.19 \pm 0.16$	5.50	$-0.17 \pm 0.38 \pm 0.13$	10.50	$+0.32 \pm 0.78 \pm 0.38$
0.75	$+0.12 \pm 0.20 \pm 0.13$	5.75	$-0.19 \pm 0.39 \pm 0.13$	10.75	$+0.35 \pm 0.83 \pm 0.41$
1.00	$+0.09 \pm 0.21 \pm 0.11$	6.00	$-0.24 \pm 0.40 \pm 0.13$	11.00	$+0.42 \pm 0.85 \pm 0.42$
1.25	$-0.06 \pm 0.22 \pm 0.09$	6.25	$-0.29 \pm 0.42 \pm 0.14$	11.25	$+0.53 \pm 0.88 \pm 0.43$
1.50	$-0.25 \pm 0.22 \pm 0.09$	6.50	$-0.30 \pm 0.45 \pm 0.14$	11.50	$+0.64 \pm 0.92 \pm 0.43$
1.75	$-0.37 \pm 0.23 \pm 0.11$	6.75	$-0.30 \pm 0.47 \pm 0.13$	11.75	$+0.74 \pm 0.96 \pm 0.42$
2.00	$-0.47 \pm 0.23 \pm 0.12$	7.00	$-0.27 \pm 0.48 \pm 0.12$	12.00	$+0.81 \pm 1.01 \pm 0.41$
2.25	$-0.50 \pm 0.25 \pm 0.12$	7.25	$-0.20 \pm 0.49 \pm 0.10$	12.25	$+0.87 \pm 1.06 \pm 0.40$
2.50	$-0.44 \pm 0.27 \pm 0.13$	7.50	$-0.10 \pm 0.51 \pm 0.10$	12.50	$+0.95 \pm 1.11 \pm 0.38$
2.75	$-0.33 \pm 0.29 \pm 0.15$	7.75	$+0.01 \pm 0.53 \pm 0.12$	12.75	$+1.04 \pm 1.15 \pm 0.38$
3.00	$-0.26 \pm 0.30 \pm 0.16$	8.00	$+0.11 \pm 0.55 \pm 0.12$	13.00	$+1.15 \pm 1.19 \pm 0.38$
3.25	$-0.14 \pm 0.30 \pm 0.16$	8.25	$+0.16 \pm 0.58 \pm 0.13$	13.25	$+1.26 \pm 1.23 \pm 0.39$
3.50	$+0.01 \pm 0.29 \pm 0.14$	8.50	$+0.18 \pm 0.61 \pm 0.14$	13.50	$+1.38 \pm 1.26 \pm 0.40$
3.75	$+0.08 \pm 0.29 \pm 0.12$	8.75	$+0.26 \pm 0.63 \pm 0.17$	13.75	$+1.49 \pm 1.30 \pm 0.42$
4.00	$+0.05 \pm 0.30 \pm 0.11$	9.00	$+0.37 \pm 0.64 \pm 0.20$	14.00	$+1.60 \pm 1.35 \pm 0.44$
4.25	$-0.03 \pm 0.31 \pm 0.11$	9.25	$+0.46 \pm 0.65 \pm 0.23$	14.25	$+1.70 \pm 1.39 \pm 0.47$
4.50	$-0.10 \pm 0.33 \pm 0.12$	9.50	$+0.50 \pm 0.66 \pm 0.26$	14.50	$+1.80 \pm 1.45 \pm 0.49$
4.75	$-0.16 \pm 0.35 \pm 0.13$	9.75	$+0.47 \pm 0.68 \pm 0.28$	14.75	$+1.90 \pm 1.50 \pm 0.51$
				15.00	$+1.99 \pm 1.56 \pm 0.53$

11 Conclusion

From a sample of 1620 B_s^0 candidates with a purity of 22%, all values of Δm_s below 3.9 ps^{-1} and between 6.5 and 8.8 ps^{-1} are excluded at 95% CL using the amplitude method. This is the first time that non-leptonic $B_s^0 \to D_s^- + X$ decays are used to search for B_s^0 oscillations. With the same sample, the B_s^0 lifetime is measured to be $1.47 \pm 0.14(\text{stat}) \pm 0.08(\text{syst})$ ps, superseding the previous measurement [16] obtained using D_s^-–hadron correlations recorded from 1991 to 1993. This new measurement is more accurate than any other single published measurement [32–34], except for the ALEPH result based on D_s^--lepton events [5].

This analysis is statistically independent of the ALEPH D_s^--lepton analysis [5]. Taking into account the correlated systematic uncertainties, the combined ALEPH results are

$$\Delta m_s > 7.9\,\text{ps}^{-1} \text{ at } 95\%\,\text{CL}$$

and

$$\tau_s = 1.51 \pm 0.11\,\text{ps}\,,$$

based on a total of 1897 $B_s^0 \to D_s^- + X$ candidates with an average purity of 28%. The combined Δm_s analysis presented here is more sensitive than previously published analyses [3,4,7,8], and also yields the highest 95% CL lower limit on the $B_s^0 - \bar{B}_s^0$ oscillation frequency.

Acknowledgements. It is a pleasure to thank our colleagues in the accelerator divisions of CERN for the excellent performance of LEP. Thanks are also due to the technical personnel of the collaborating institutions for their support in constructing and maintaining the ALEPH experiment. Those of us not from member states wish to thank CERN for its hospitality.

References

1. J.M. Flynn and C.T. Sachrajda, *Heavy quark physics from lattice QCD*, hep-lat/9710057, to appear in Heavy Flavours (2^{nd} edition), ed. A.J. Buras and M. Linder, World Scientific, Singapore
2. O. Schneider, *Heavy quark spectroscopy, lifetimes and oscillations*, CERN–PPE/97–143, to appear in the proceedings of the 18^{th} International Symposium on Lepton-Photon Interactions, Hamburg, Germany, July 1997
3. ALEPH Collaboration, *An investigation of* B_d^0 *and* B_s^0 *oscillation*, Phys. Lett. B **322** (1994) 441
4. ALEPH Collaboration, *Limit on* B_s^0 *oscillation using a jet charge method*, Phys. Lett. B **356** (1995) 409
5. ALEPH Collaboration, *Study of the* $B_s^0 - \bar{B}_s^0$ *oscillation frequency using* $D_s^- \text{–} \ell^+$ *combinations in Z decays*, Phys. Lett. B **377** (1996) 205
6. ALEPH Collaboration, *Combined limit on* B_s^0 *oscillations*, PA08–020, contribution to the 28^{th} International Conference on High Energy Physics, Warsaw, Poland, July 1996; *Search for* B_s^0 *oscillations using inclusive leptons events*, EPS–612, contribution to the International Europhysics Conference on High Energy Physics, Jerusalem, Israel, August 1997
7. DELPHI Collaboration, *Search for* $B_s^0 - \bar{B}_s^0$ *oscillations*, Phys. Lett. B **414** (1997) 382; *Search for* $B_s^0 - \bar{B}_s^0$ *oscillations and measurement of the* B_s^0 *lifetime*, EPS–457, contribution to the International Europhysics Conference on High Energy Physics, Jerusalem, Israel, August 1997
8. OPAL Collaboration, *A study of* B *meson oscillations using hadronic* Z *decays containing leptons*, Z. Phys. C **76** (1997) 401; *An updated study of* B *meson oscillations using dilepton events*, Z. Phys. C **76** (1997) 417; *Investigation of the* B_s^0 *oscillation frequency using* $\phi\ell$ *and* $D_s\ell$ *correlations*, PA08–014, contribution to the 28^{th} International Conference on High Energy Physics, Warsaw, Poland, July 1996.
9. ALEPH Collaboration, *ALEPH: a detector for electron-positron annihilations at LEP*, Nucl. Instrum. Methods A **294** (1990) 121;
   B. Mours et al., Nucl. Instrum. Methods A **379** (1996) 101
10. ALEPH Collaboration, *Performance of the ALEPH detector at LEP*, Nucl. Instrum. Methods A **360** (1995) 481
11. ALEPH Collaboration, *Improved measurements of electroweak parameters from* Z *decays into fermion pairs*, Z. Phys. C **53** (1992) 1
12. T. Sjöstrand and M. Bengtsson, Computer Phys. Commun. **43** (1987) 367
13. J. Körner and G. Schuler, Z. Phys. C **38** (1988) 511
14. ALEPH Collaboration, *A precise measurement of* $\Gamma(Z \to b\bar{b})/\Gamma(Z \to \textit{hadrons})$, Phys. Lett. B **313** (1993) 535
15. ALEPH Collaboration, *Heavy quark tagging with leptons in the ALEPH detector*, Nucl. Instrum. Methods A **346** (1994) 461
16. ALEPH Collaboration, *Measurement of* D_s^+ *meson production in* Z *decays and of the* $\bar{B}_s^0$ *lifetime*, Z. Phys. C **69** (1995) 585
17. CLEO Collaboration, *Measurements of* $B \to D_s^+ X$ *decays*, Phys. Rev. D **53** (1996) 4734
18. A. Rosado-Schlosser, *Lebensdauerbestimmung von* B_s^0*-Mesonen mit dem ALEPH-Detektor*, Ph.D. thesis, MPI–PhE/97–17, Ludwig-Maximilians Universität, Munich, 1997
19. R.M. Barnett et al., Particle Data Group, Phys. Rev. D **54** (1996) 1
20. ALEPH, DELPHI, L3, OPAL Collaborations and the SLD Heavy Flavour Group, *A combination of preliminary electroweak measurements and constraints on the Standard Model*, CERN–PPE/96–183
21. ALEPH, DELPHI, L3, OPAL Collaborations, *Combining heavy flavour electroweak measurements at LEP*, Nucl. Instrum. Methods A **378** (1996) 101
22. CLEO Collaboration, *Charm production in nonresonant* e^+e^- *annihilations at* $\sqrt{s} = 10.55\,GeV$, Phys. Rev. D **37** (1988) 1719, erratum **39** (1989) 1471;
    OPAL Collaboration, *A study of charm hadron production in* $Z \to c\bar{c}$ *and* $Z \to b\bar{b}$ *decays at LEP*, Z. Phys. C **72** (1996) 1;
    DELPHI Collaboration, *Update of the measurement of* $R_c P_{c\to D_s}$ *and* $R_b P_{b\to D_s}$ *using inclusive* $D_s^- \to \phi\pi^-$ *and* $D_s^- \to K^{*0}K^-$ *channels*, PA01–030, contribution to the 28^{th} International Conference on High Energy Physics, Warsaw, Poland, July 1996
23. ARGUS Collaboration, *Production of* D_s^+ *mesons in* B *decays and determination of* f_{D_s}, Z. Phys. C **54** (1992) 1
24. CLEO Collaboration, *Exclusive and inclusive decays of* B *mesons into* D_s^- *mesons*, Phys. Rev. Lett. **64** (1990) 2117
25. CLEO Collaboration, D_s^-*-lepton charge correlations in* B *meson decays: a study of the* D_s^- *meson production mechanism*, EPS–0169, contribution to the International Europhysics Conference on High Energy Physics, Brussels, Belgium, July 1995
26. ALEPH Collaboration, *Measurement of the* B_s^0 *lifetime*, Phys. Lett. B **322** (1994) 275
27. ALEPH Collaboration, *Measurement of* $B - \bar{B}$ *mixing at the* Z *using a jet charge method*, Phys. Lett. B **284** (1992) 177
28. M.R. Adams et al., Phys. Rev. D **50** (1994) 1836
29. M. Beneke, G. Buchalla, I. Dunietz, Phys. Rev. D **54** (1996) 4419
30. ALEPH Collaboration, *Measurement of the effective* b *quark fragmentation function at the* Z *resonance*, Phys. Lett. B **357** (1995) 699
31. H.-G. Moser and A. Roussarie, Nucl. Instrum. Methods A **384** (1997) 491
32. CDF Collaboration, *Measurement of the* B_s^0 *meson lifetime*, Phys. Rev. Lett. **74** (1995) 4988; *Measurement of the lifetime of the* B_s^0 *meson using the exclusive decay mode* $B_s^0 \to J/\psi\phi$, Phys. Rev. Lett. **77** (1996) 1945
33. DELPHI Collaboration, *Mean lifetime of the* B_s^0 *meson*, Z. Phys. C **71** (1996) 11
34. OPAL Collaboration, *An improved measurement of the* B_s^0 *lifetime*, Phys. Lett. B **350** (1995) 273; *A measurement of the* B_s^0 *lifetime using reconstructed* D_s^- *mesons*, CERN–PPE/97–095, submitted to Z. Phys. C